

ROBUST PRECONDITIONING OF MIXED-DIMENSIONAL PDES ON 3D-1D DOMAINS COUPLED WITH LAGRANGE MULTIPLIERS

NUNZIO DIMOLA[†], MIROSLAV KUČHTA^{*}, KENT-ANDRE MARDAL[‡], AND PAOLO ZUNINO[†]

ABSTRACT. In the context of micro-circulation, the coexistence of two distinct length scales - the vascular radius and the tissue/organ scale - with a substantial difference in magnitude, poses significant challenges. To handle slender inclusions and simplify the geometry involved, a technique called *topological dimensionality reduction* is employed, which suppresses manifold dimensions associated with the smaller characteristic length. However, the resulting discretized system's algebraic structure presents a challenge in constructing efficient solution algorithms. This chapter addresses this challenge by developing a robust preconditioner for the 3d-1d problem using the operator preconditioning technique. Robustness of the preconditioner is demonstrated with respect to problem parameters, except for the vascular radius. The vascular radius, as demonstrated, plays a fundamental role in mathematical well-posedness of the problem and the preconditioner's effectiveness.

1. INTRODUCTION

The human cardiovascular system displays a diverse range of scales and characteristics, encompassing major blood vessels, arterioles, and capillaries, with diameters ranging from several cm to a few μm . In particular, when examining the microcirculation, the challenge intensifies due to the substantial disparity in scale between the diameter of small vessels (μm) and the size of the corresponding system or organ they supply (dm). To cope with this disparity, intricate vascular networks that occupy space are needed, leading to complex geometric structures.

Due to the inherent complexities involved, simulating the flow throughout the entire cardiovascular system is not practical or applicable. However, it is crucial to adopt a comprehensive approach that incorporates interactions between different system components by integrating models operating at various levels of detail. This approach is commonly referred to as *geometrical multi-scale* or *hybrid-dimensional modeling*.

Two types of hybrid dimensional models can be considered: sequential and embedded. In an embedded multiscale model, components of varying levels of detail are integrated within the same domain. A prime example is the micro-circulation, where a complex vascular network comprising arterioles, capillaries, and small veins exists within the biological tissue.

From the modeling standpoint, such ideas have appeared in the past three decades, (at least), for modeling wells in subsurface reservoirs in [33, 34] and for modeling microcirculation in [2, 10, 11, 39, 14]. A similar approach has been recently used to model soil/root interactions [17]. However, these application-driven seminal ideas were not followed by a systematic theory and rigorous mathematical analysis. At the same time the models introduce additional mathematical complexity, in particular concerning the functional setting for the solution as it involves coupling PDEs on domains with high dimensionality gap. Such mathematical challenge has recently attracted the attention of many researchers. The sequence of works by [7, 8, 9], followed by [26, 25, 22], have remedied the well-posedness by weakening the regularity assumptions that define a solution.

[†]MOX, DEPARTMENT OF MATHEMATICS, POLITECNICO DI MILANO, ITALY

^{*}SIMULA RESEARCH LABORATORY, OSLO, NORWAY

[‡]DEPARTMENT OF MATHEMATICS, UNIVERSITY OF OSLO, NORWAY

E-mail addresses: nunzio.dimola@polimi.it, miroslav@simula.no, kent-and@math.uio.no, paolo.zunino@polimi.it.

Submitted to *Quantitative approaches to microcirculation: mathematical models, computational methods, measurements and data analysis (SEMA/SIMAI Collection on Microcirculation)*.

Nevertheless, the mathematical understanding of embedded, mixed-dimensional problems is not sufficient to successfully apply these models to realistic problems. An essential difficulty to overcome is the development of efficient numerical solvers that can handle the large separation of spatial scales between the domains of the equations and the subsequent geometrical complexity of the vascular network.

Actually, the study of the interplay between the mathematical structure of the problem and solvers, as well as preconditioners for its discretization is still in its infancy. The results presented in [24] for the solution of $1d$ differential equations embedded in $2d$, and more recently extended to the $3d-1d$ case in [23], have paved the way, but a lot more has to be understood. This work proceeds along this direction, with the aim to discuss the main mathematical challenges at the basis of the development of optimal solvers of mixed-dimensional $3d-1d$ problems coupled by Lagrange multipliers.

We model the case of one single small vessel by the domain $\Omega \subset \mathbb{R}^3$ that is an open, connected and convex set that can be subdivided in two parts, Ω_\ominus and $\Omega_\oplus = \Omega \setminus \overline{\Omega_\ominus}$ representing respectively the vessel and the tissue. Let Ω_\ominus be a *generalized cylinder* that is the swept volume of a two dimensional set, $\partial\mathcal{D}$, moved along a curve, Λ , in the three-dimensional domain, Ω , see Figure 1 for an illustration. For dimensional reduction of the vessel domain we finally assume that $|\mathcal{D}| \ll |\Lambda|$.

With the purpose of developing robust preconditioners for the $3d-1d$ problem arising from microcirculation, let us consider a prototype problem that originates from coupling of two $3d$ diffusion equations:

$$\begin{aligned} -\kappa_\oplus \Delta u_\oplus &= f && \text{in } \Omega_\oplus, \\ -\kappa_\ominus \Delta u_\ominus &= f && \text{in } \Omega_\ominus, \\ u_\oplus - u_\ominus &= g && \text{on } \Gamma_\varepsilon, \\ \kappa_\oplus \nabla u_\oplus \cdot \nu_{\Gamma_\varepsilon} - \kappa_\ominus \nabla u_\ominus \cdot \nu_{\Gamma_\varepsilon} &= 0 && \text{on } \Gamma_\varepsilon, \\ u_\oplus, u_\ominus &= 0 && \text{on } \partial\Omega. \end{aligned} \tag{1}$$

Here, u_\oplus and u_\ominus are the unknowns, and $\kappa_\oplus > 0$ and $\kappa_\ominus > 0$ are the diffusivities in the two different domains which we shall in the following assume to be constant for the sake of simplicity. Further, $\Gamma_\varepsilon = \partial\Omega_\oplus \cap \partial\Omega_\ominus$ where $\varepsilon = \text{diam}\mathcal{D}$ denotes the diameter of the $2d$ transversal cross sections of Ω_\ominus . Finally, f is a forcing term defined in the whole Ω . We remark that the coupling condition $u_\oplus - u_\ominus = g$ on Γ_ε is of Dirichlet type. In this sense our starting point differs from the more commonly studied problem (see the seminal paper [9]) which considers the Robin coupling, i.e. modeling the flux at the interface as $-\kappa_\oplus \nabla u_\oplus \cdot \nu_{\Gamma_\varepsilon} = \gamma(u_\oplus - u_\ominus)$ on Γ_ε . However, viewing the latter as a perturbation of the Dirichlet condition, our setting is relevant also for the Robin coupling, see [3].

By applying a suitable model reduction strategy to (1), which exploits the following transverse averages as already described in [26],

$$\overline{w}(s) = |\partial\mathcal{D}(s)|^{-1} \int_{\partial\mathcal{D}(s)} w d\gamma \quad \text{and} \quad \overline{\overline{w}}(s) = |\mathcal{D}(s)|^{-1} \int_{\mathcal{D}(s)} w d\sigma,$$

we obtain the $3d-1d$ coupled problem of the form

$$\begin{aligned} -\kappa \Delta u + \varepsilon p_\ominus \delta_\Lambda &= f && \text{in } \Omega, \\ -\varepsilon^2 \kappa_\ominus d_s^2 u_\ominus - \varepsilon p_\ominus &= \varepsilon^2 \overline{\overline{f}} && \text{on } \Lambda, \\ \varepsilon(\overline{\mathcal{T}}_\Lambda u - u_\ominus) &= g && \text{on } \Lambda, \\ u &= 0 && \text{on } \partial\Omega, \\ u_\ominus &= 0 && \text{on } \partial\Lambda. \end{aligned} \tag{2}$$

Here $\kappa = \kappa_\oplus$ in Ω_\oplus and $\kappa_\ominus = \overline{\kappa_\ominus}$ on Λ being the centerline of Ω_\ominus . Throughout the paper we will use the subscript \ominus , e.g. u_\ominus , for functions on Λ (and, in general, on domains with topological dimension smaller than that of the ambient space) while functions on Ω are denoted, as usual, by italic lower case letters. Here, the primal unknowns are u and u_\ominus , while the unknown p_\ominus is the Lagrange multiplier used to enforce the coupling of u and u_\ominus . Furthermore, δ_Λ is a Dirac

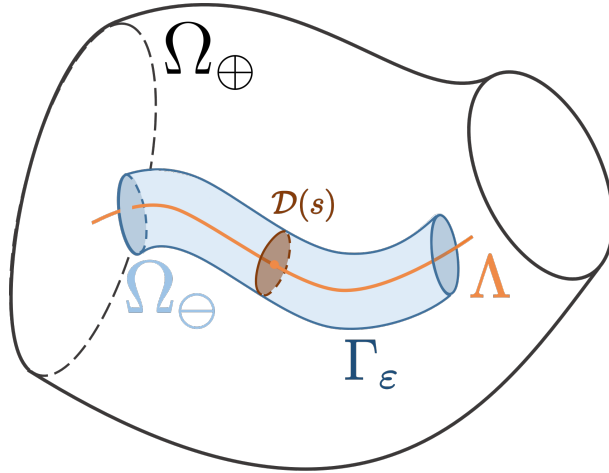


FIGURE 1. Geometrical setting considered in this paper, and the associated notation. Domain Ω_\ominus is assumed to be a slender generalized cylinder characterized by the centerline Λ parameterized by the arclength coordinate s and $2d$ transversal cross section $\mathcal{D}(s)$.

delta function. The operator obtained from a combination of the average operator $\overline{(\cdot)}$ with the trace on Γ_ε will be denoted with $\overline{\mathcal{T}}_\Lambda = \overline{(\cdot)} \circ \mathcal{T}_\Gamma$, as it maps functions on Ω to functions on Λ . Note that $\overline{\mathcal{T}}_\Lambda$ thus implicitly depends on ε .

Because of the high dimensional gap between $3d$ and $1d$, and the presence of singularities in the solution u due to the $1d$ coupling, the well-posedness of the problem (2) is challenging [9, 8]. In the context of Robin coupling conditions at the $3d$ - $1d$ interface, the singularity is addressed in a number of works e.g. by proposing a splitting strategy where the singularity is captured by Green's functions [13], regularizing the problem by distributing the singular source term on the coupling surface or in the bulk [19, 18] or deriving error estimates in tailored norms [20, 8]. For these formulations efficient solution algorithms have been developed utilizing algebraic multigrid [16, 6] or fast Fourier transform for preconditioning [27].

While the Robin coupling typically leads to elliptic problems, enforcing the Dirichlet coupling in (2) by Lagrange multiplier yields a saddle point system. Here, as recently shown in [22], the high $3d$ - $1d$ dimensional gap requires the multiplier to reside in fractional order Sobolev spaces on Λ in order to obtain well-posedness. However, scalable solvers for the resulting linear systems are currently lacking. Here we aim to address this issue by constructing robust block-diagonal preconditioners for (2) within the framework of operator preconditioning [30]. In particular, to obtain robust estimates we establish well-posedness of the coupled problem in weighted, fractional Hilbert spaces.

The structure of the chapter is outlined as follows. We start with the analysis of the coupled problem in Section 2. Next, we investigate the performance of the resulting preconditioner in Section 3, leading us to the observation that the parameter ε in (2) assumes a distinctive role beyond that of a standard material parameter. This unique role is further examined in Section 4, where we establish a close connection between ε and the well-posedness of the coupled problem. Finally, we provide our conclusions in Section 5.

2. MATHEMATICAL FORMULATION OF THE $3d$ - $1d$ COUPLED PROBLEM

Before delving into the precise mathematical formulation of problem (2), we will introduce some fundamental notation. Let D represent a bounded domain in \mathbb{R}^d , where $d = 1, 2, 3$. In this context, $L^2(D)$ denotes the space of functions that are square integrable over D , while $H^k(D)$ refers to the space of functions possessing k derivatives in L^2 . We denote the closure of $C_0^\infty(D)$ in $H^k(D)$ as $H_0^k(D)$. When the context is clear, we may simplify the notation by using H^k instead of $H^k(D)$. For a Hilbert space $X = X(D)$ with its corresponding dual space X' , the norm and associated inner products are denoted as $\|\cdot\|_X$ and $(\cdot, \cdot)_X$, respectively. The duality pairing is represented by $\langle \cdot, \cdot \rangle_X$, and if necessary, we will explicitly indicate the underlying domain by

using $(\cdot, \cdot)_D$ and $\langle \cdot, \cdot \rangle_D$. With a slight abuse of notation, the dual of H^k is H^{-k} for $k \in \mathbb{R}$. Similarly, H_0^{-k} is the dual of H_0^k . We will use scaled and intersected inner products, norms and Hilbert spaces for our analysis of robustness. For instance $\varepsilon H_0^1(D)$ is defined in terms of the inner product

$$(u, v)_{\varepsilon H_0^1(D)} = \varepsilon^2 (\nabla u, \nabla v)_{L^2(D)}.$$

Notice that with this definition, the norm scales linearly in ε , i.e.,

$$\|u\|_{\varepsilon H_0^1} = \varepsilon \|u\|_{H_0^1}.$$

The intersection of two Hilbert spaces X and Y is denoted $X \cap Y$ and has an inner product

$$(x, y)_{X \cap Y} = (x, y)_X + (x, y)_Y.$$

We can now formulate precisely the weak formulation of problem (2) that will be considered in this paper. The problem reads: Find $u \in V, u_\circ \in V_\circ, p_\circ \in Q_\circ$ such that

$$\begin{aligned} a([u, u_\circ], [v, v_\circ]) + b([v, v_\circ], p_\circ) &= \langle f, [v, v_\circ] \rangle_\Omega \quad \forall [v, v_\circ] \in [V, V_\circ] \\ b([u, u_\circ], q_\circ) &= \langle g, q_\circ \rangle_\Lambda \quad \forall q_\circ \in Q_\circ. \end{aligned} \quad (3)$$

with

$$\begin{aligned} a([u, u_\circ], [v, v_\circ]) &= \kappa (\nabla u, \nabla v)_{L^2(\Omega)} + \kappa_\circ \varepsilon^2 (d_s u_\circ, d_s v_\circ)_{L^2(\Lambda)}, \\ b([v, v_\circ], q_\circ) &= \varepsilon \langle \overline{\mathcal{T}}_\Lambda v - v_\circ, q_\circ \rangle_\Lambda \end{aligned}$$

and $V = \kappa^{1/2} H_0^1(\Omega)$, $V_\circ = \kappa_\circ^{1/2} \varepsilon H_0^1(\Lambda)$, and $Q_\circ = \kappa^{-1/2} \varepsilon H^{-\frac{1}{2}}(\Lambda) \cap \kappa_\circ^{-1/2} H^{-1}(\Lambda)$. We remark that a main difference between [22] and the functional setting considered here is that the Lagrange multiplier space Q_\circ is a weighted intersection space $\kappa^{-1/2} \varepsilon H^{-\frac{1}{2}}(\Lambda) \cap \kappa_\circ^{-1/2} H^{-1}(\Lambda)$ rather than $H^{-\frac{1}{2}}(\Lambda)$. This choice is fundamental for the development of robust preconditioners, as will be motivated later on.

2.1. The stability of the continuous problem. We show well-posedness of the variational problem (3) in space $X = V \times V_\circ \times Q_\circ$ considered with its canonical norms by applying the abstract Brezzi theory [4]. To this end we let

$$\begin{aligned} A : (V \times V_\circ) &\rightarrow (V \times V_\circ)', \quad \langle A[u, u_\circ], [v, v_\circ] \rangle_{V \times V_\circ} = a([u, u_\circ], [v, v_\circ]), \\ B : (V \times V_\circ) &\rightarrow Q_\circ', \quad \langle B[u, u_\circ], q_\circ \rangle_{Q_\circ} = b([u, u_\circ], q_\circ), \end{aligned}$$

such that (3) can be equivalently stated as: Find $x = [u, u_\circ, p_\circ] \in X$ such that

$$\mathcal{A}x = f \text{ in } X', \quad \mathcal{A} = \begin{pmatrix} A & B' \\ B & 0 \end{pmatrix}.$$

The operator $\mathcal{A} : X \rightarrow X'$ is then an isomorphism (equivalently (3) is well-posed) provided that it satisfies the four Brezzi conditions, namely, the operators A and B are bounded, A is coercive on the $\ker B \subset V \times V_\circ$ and B satisfies the inf-sup condition.

Of the four Brezzi conditions required for problem (3), the coercivity and boundedness of A were established in [22] in the setting required here ($V \times V_\circ$ are the same and only Q_\circ has changed) and will therefore not be repeated. Hence, we only need to verify the properties of the B operator.

Theorem 2.1. $b(\cdot, \cdot) : [V, V_\circ] \times Q_\circ \rightarrow \mathbb{R}$ satisfies the following conditions:

$$b([u, u_\circ], q_\circ) \leq C_B \| [u, u_\circ] \|_{[V, V_\circ]} \| q_\circ \|_{Q_\circ}, \quad u \in V, u_\circ \in V_\circ, q_\circ \in Q_\circ, \quad (4)$$

$$\sup_{[u, u_\circ] \in [V, V_\circ]} \frac{b([u, u_\circ], q_\circ)}{\| [u, u_\circ] \|_{[V, V_\circ]}} \geq \beta \| q_\circ \|_{Q_\circ}, \quad q_\circ \in Q_\circ \quad (5)$$

with positive constants C_B, β .

Proof. We recall that owing to Dirichlet boundary conditions for u , u_\circ we have the equivalence between the seminorms (induced by A) and the full H^1 norms. In [22] the following was established:

$$\varepsilon \|\overline{\mathcal{T}}_\Lambda u\|_{H^{1/2}(\Lambda)} \leq C_{\mathcal{T}} \|\mathcal{T}_{\Gamma_\varepsilon} u\|_{H^{1/2}(\Gamma_\varepsilon)} \leq C \|u\|_{H^1(\Omega)}, \quad \forall u \in H^1(\Omega),$$

where constants $C_{\mathcal{T}}$ and C are independent from ε . Hence, the boundedness of $b(\cdot, \cdot)$ can be obtained in a direct way as:

$$\begin{aligned} b([u, u_\circ], q_\circ) &= \varepsilon \langle \overline{\mathcal{T}}_\Lambda u - u_\circ, q_\circ \rangle_\Lambda \\ &\leq \varepsilon |\langle \overline{\mathcal{T}}_\Lambda u, q_\circ \rangle_\Lambda| + \varepsilon |\langle u_\circ, q_\circ \rangle_\Lambda| \\ &\leq \|\overline{\mathcal{T}}_\Lambda u\|_{H^{1/2}(\Lambda)} \varepsilon \|q_\circ\|_{H^{-1/2}(\Lambda)} + \varepsilon \|u_\circ\|_{H^1(\Lambda)} \|q_\circ\|_{H^{-1}(\Lambda)} \\ &= \kappa^{1/2} \varepsilon \|\overline{\mathcal{T}}_\Lambda u\|_{H^{1/2}(\Lambda)} \kappa^{-1/2} \|q_\circ\|_{H^{-1/2}(\Lambda)} + \varepsilon \kappa_\circ^{1/2} \|u_\circ\|_{H^1(\Lambda)} \kappa_\circ^{-1/2} \|q_\circ\|_{H^{-1}(\Lambda)} \\ &\leq \kappa^{1/2} C \|u\|_{H^1(\Omega)} \kappa^{-1/2} \|q_\circ\|_{H^{-1/2}(\Lambda)} + \varepsilon \kappa_\circ^{1/2} \|u_\circ\|_{H^1(\Lambda)} \kappa_\circ^{-1/2} \|q_\circ\|_{H^{-1}(\Lambda)} \\ &\leq C_B (\|u\|_V^2 + \|u_\circ\|_{V_\circ}^2)^{1/2} \|q_\circ\|_{Q_\circ}. \end{aligned}$$

Next, the inf-sup condition reads

$$\sup_{[u, u_\circ] \in [V, V_\circ]} \frac{\varepsilon \langle \overline{\mathcal{T}}_\Lambda u - u_\circ, q_\circ \rangle_\Lambda}{(\|u\|_{\sqrt{\kappa}H^1(\Omega)}^2 + \varepsilon^2 \|u_\circ\|_{\sqrt{\kappa_\circ}H^1(\Lambda)}^2)^{1/2}} \geq \beta \|q_\circ\|_{Q_\circ}.$$

We first note that $(\alpha X)' = \alpha^{-1} X'$ holds for dual of weighted Hilbert space. In turn, let R_1 be the Riesz map from $\kappa_\circ^{-1/2} H^{-1}$ to $\kappa_\circ^{1/2} H^1$ and $R_{1/2}$ be the Riesz map from $\kappa^{-1/2} H^{-1/2}$ to $\kappa^{1/2} H^{1/2}$. Then $\hat{u}_\circ = -\frac{1}{\varepsilon} R_1 q_\circ$ implies that $\varepsilon \|\hat{u}_\circ\|_{\sqrt{\kappa_\circ}H^1} = \|q_\circ\|_{\kappa_\circ^{-1/2}H^{-1}}$. From [22], we also have that there exists a harmonic extension operator H such that for $\hat{u} = H\hat{q}_\circ$, $\hat{q}_\circ \in H^{1/2}$. Letting $\hat{q}_\circ = R_{1/2} q_\circ$ we obtain that $\hat{q}_\circ = \overline{\mathcal{T}}_\Lambda \hat{u}$ where $\|\hat{q}_\circ\|_{\sqrt{\kappa}H^{1/2}} = \|q_\circ\|_{\kappa^{-1/2}H^{-1/2}}$ and

$$\|\hat{u}\|_{H^1(\Omega)} \leq C_{IT} \varepsilon \|\hat{q}_\circ\|_{H^{\frac{1}{2}}(\Gamma_\varepsilon)} = \varepsilon C_{IT} \|q_\circ\|_{H^{-\frac{1}{2}}(\Gamma_\varepsilon)}.$$

We note that the latter inequality, generally named the *inverse trace inequality*, involves the generic constant C_{IT} that may possibly depend on the domain Γ_ε and precisely on its cross section quantified by the (small) parameter ε . Hence, we obtain

$$\begin{aligned} \sup_{[u, u_\circ] \in [V, V_\circ]} \frac{\varepsilon \langle \overline{\mathcal{T}}_\Lambda u - u_\circ, q_\circ \rangle_\Lambda}{(\|u\|_{\sqrt{\kappa}H^1(\Omega)}^2 + \varepsilon^2 \|u_\circ\|_{\sqrt{\kappa_\circ}H^1(\Lambda)}^2)^{1/2}} &\geq \frac{\varepsilon \langle \overline{\mathcal{T}}_\Lambda \hat{u} - \hat{u}_\circ, q_\circ \rangle_\Lambda}{(\|\hat{u}\|_{\sqrt{\kappa}H^1(\Omega)}^2 + \varepsilon^2 \|\hat{u}_\circ\|_{\sqrt{\kappa_\circ}H^1(\Lambda)}^2)^{1/2}} \\ &\geq \frac{\varepsilon (\langle R_{1/2} q_\circ, q_\circ \rangle + \langle \frac{1}{\varepsilon} R_1 q_\circ, q_\circ \rangle)}{(C_{IT} \varepsilon^2 \|q_\circ\|_{\kappa^{-1/2}H^{-1/2}(\Lambda)}^2 + \|q_\circ\|_{\kappa_\circ^{-1/2}H^{-1}(\Lambda)}^2)^{1/2}} \geq \beta \|q_\circ\|_{Q_\circ}. \end{aligned}$$

□

It is noteworthy that a proper choice of weighted-intersected Sobolev spaces has led to removal of any *explicit* dependence of the inf-sup constant β on κ , κ_\circ and ε . On the other hand, caution is needed as, through possible dependence of C_{IT} on ε , the radius may influence β , and in turn robustness of the estimates in ε .

2.2. Numerical evidence about preconditioning the mixed-dimensional problems.

The exploitation of iterative solvers, such as Krylov methods, is crucial to obtain fast solution algorithms for the discretized problems, yet, their performance essentially depends on existence of (a practical) preconditioner which improves spectral properties of the linear systems [38]. In constructing preconditioners for the 3d-1d-problems, a main objective is to establish a parameter robustness preconditioner, i.e. a preconditioner with performance that does not deteriorate with respect to discretization parameters (mesh and element sizes), variations in material parameters ($\kappa > 0$, $\kappa_\circ > 0$) as well as the geometrical parameter ε , crucial for 3d-1d problems. As an example, in the context of 3d-1d microcirculation model (2), the vessel radius appears explicitly

and implicitly in the $3d-1d$ problem formulation, as the residue of the bridging of the three-dimensional topology to the one-dimensional one. Then, it must be taken into account.

Here we wish to construct robust preconditioners for the coupled $3d-1d$ problem (3) which induces an operator equation: Find $x = [u, u_\odot, p_\odot] \in X$ such that

$$\mathcal{A}x = f \text{ in } X', \quad \mathcal{A} := \begin{pmatrix} -\kappa\Delta & & \varepsilon\overline{\mathcal{T}}_\Lambda' \\ & -\kappa_\odot\varepsilon^2\Delta_\Lambda & -\varepsilon I \\ \varepsilon\overline{\mathcal{T}}_\Lambda & & 0 \end{pmatrix}, \quad (6)$$

where, for a one-dimensional manifold as Λ , the operator Δ_Λ is equivalent to second derivative in the direction tangent to Λ , previously denoted as d_s^2 .

To establish the preconditioners we follow the framework of operator preconditioning [30]. That is, having shown stability of (3) we define the preconditioner as a Riesz map $\mathcal{B} : X' \rightarrow X$ with respect to inner products/norms in which the problem was shown to be well-posed. In turn, the framework relates the conditioning of the (preconditioned) operator $\mathcal{B}\mathcal{A} : X \rightarrow X$ to the stability constants of the Brezzi theory. More precisely, independence of the constants with respect to a particular problem parameter translates to robustness of the preconditioner (in the said parameter variations). Note that in case of (3), the critical Brezzi constants are C_B and β related to the boundedness and inf-sup condition of the bilinear form b , cf. Theorem 2.1. We remark that to obtain a robust discrete preconditioner, stable discretization is required in addition to well-posedness of the continuous problem. In particular, the Brezzi constants of the discretized problem must be independent of the discretization parameter.

Applying operator preconditioning, the analysis of well-posedness in [22] and Theorem 2.1 yields to two different preconditioners for (6). Here, a key difference is the construction of the multiplier space, as [22] consider $H^{-1/2}(\Lambda)$. However this space does not lead to robust algorithms as we shall demonstrate next. In fact, intersection spaces of Theorem 2.1 will be needed to obtain robustness in material parameters. At the same time, at the end of this work it will become clear that the radius ε , as a parameter, plays a special and critical role in the robustness of a preconditioner stemming from Theorem 2.1.

2d-1d preconditioning example. Let us illustrate the challenges of developing a robust preconditioner for mixed-dimensional equations by using a $2d$ analogue of (6) where we let $\Lambda = \Lambda_\varepsilon$ be a closed curved contained in the interior of $\Omega \subset \mathbb{R}^2$, cf. Figure 2. Here the coupling between the problem unknowns defined on Ω and Λ shall be realized by the standard $2d-1d$ trace operator leading to the coupled problem: Find $y = [u, u_\odot, p_\odot] \in Y$ such that

$$\mathcal{A}y = f \text{ in } Y', \quad \mathcal{A} = \begin{pmatrix} -\Delta & & \mathcal{T}_\Lambda' \\ & -\kappa_\odot\Delta_\Lambda & -I \\ \mathcal{T}_\Lambda & & 0 \end{pmatrix}. \quad (7)$$

Note that (7) is structurally similar to the $3d-1d$ coupled problem (6). However, for simplicity, the model $2d-1d$ problem contains only a single parameter, $\kappa_\odot > 0$, whose value can be (arbitrarily) large or small. We also recall that Λ is closed and thus, in order to have an invertible operator on the whole of $H^1(\Lambda)$, we set $-\Delta_\Lambda = -\Delta_\Lambda + I$ in this section. We finally remark that in (6) the Laplacian on Λ is invertible due to boundary conditions imposed on $\partial\Omega_\ominus$ outside the coupling surface.

Following [24] where (7) has been shown to be well-posed with $Y = H_0^1(\Omega) \times H^1(\Lambda) \times H^{-1/2}(\Lambda)$ we shall construct preconditioners as Riesz maps with respect to two different inner products on Y leading to operators

$$\mathcal{B}_0 = \begin{pmatrix} -\Delta & & \\ & -\kappa_\odot\Delta_\Lambda & \\ & & -\Delta_\Lambda^{-1/2} \end{pmatrix}^{-1}, \quad \mathcal{B}_1 = \begin{pmatrix} -\Delta & & \\ & -\kappa_\odot\Delta_\Lambda & \\ & & -\Delta_\Lambda^{-1/2} - \kappa_\odot^{-1}\Delta_\Lambda^{-1} \end{pmatrix}^{-1}. \quad (8)$$

Here \mathcal{B}_0 stems from the analysis in [24] and can be seen to be analogous to the Riesz map preconditioner established in [22] for the coupled $3d-1d$ problem (6). In particular, the multiplier block of the preconditioner is a Riesz map of $H^{-1/2}(\Lambda)$ and is independent of the parameter

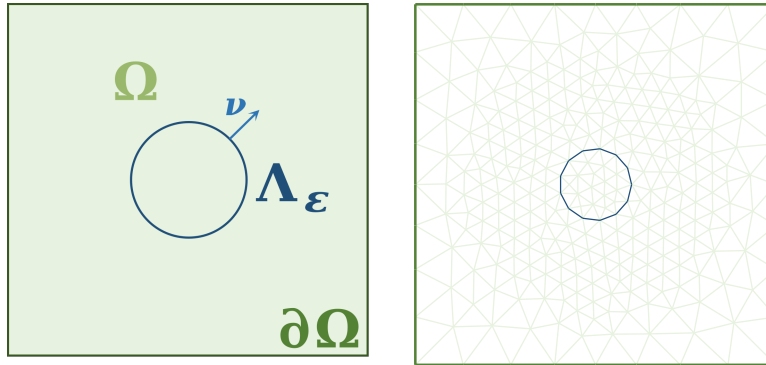


FIGURE 2. (Left) Geometrical setting of the $2d-1d$ problem (10). Domain Λ_ϵ plays similar role to the centerline in $3d-1d$ system (2). (Right) In the experiments triangulation of Ω conforms to Λ .

κ_\odot . On the other hand, with \mathcal{B}_1 the multiplier is sought in the intersection space $H^{-1/2}(\Lambda) \cap \kappa_\odot^{-1/2}H^{-1}(\Lambda)$, cf. Theorem 2.1.

We shall compare the two preconditioners in terms of their spectral condition numbers defined as the ratio between the largest and smallest in magnitude eigenvalues of the problem: Find $y \in Y$, $\lambda \in \mathbb{R}$

$$\mathcal{A}y = \lambda \mathcal{B}_1^{-1}y \quad \text{in } Y'. \quad (9)$$

To assess robustness of the preconditioners we consider the generalized eigenvalue problem (9) for different values of $10^{-8} \leq \kappa_\odot \leq 10^8$ and refinements of the domain $\Omega = (-1, 1)^2$ with $\Gamma_\epsilon = \{x \in \Omega, |x| = 0.1\}$. We then discretize the problem by continuous linear Lagrange elements (\mathbb{P}_1) where the finite element mesh of Ω always conforms to Λ , cf. Figure 2.

Before addressing the preconditioners let us briefly comment on the approximation property of the chosen discretization. To this end we note that (7) is associated with a system

$$\begin{aligned} -\Delta u &= f && \text{in } \Omega, \\ -\kappa_\odot \Delta_\Lambda u_\odot - \llbracket \nabla u \rrbracket \cdot \nu &= f_\odot && \text{on } \Lambda, \\ u - u_\odot &= g && \text{on } \Lambda \end{aligned} \quad (10)$$

which is here supplied with homogeneous Dirichlet boundary conditions for u , u_\odot on $\partial\Omega$ and $\partial\Lambda$ respectively. Here $\llbracket \cdot \rrbracket$ is the jump operator on Λ , $\llbracket v \rrbracket = v^+ - v^-$, defined with respect to the normal vector on the curve which points from the positive to the negative side.

Using (10) we measure convergence of the discrete approximations u_h , $u_{\odot,h}$, $p_{\odot,h}$ in the norms induced by the (symmetric and positive definite) operator \mathcal{B}_1^{-1} . Here, the linear systems stemming from discretization¹ by \mathbb{P}_1 elements are solved with a preconditioned MinRes solver using relative tolerance of 10^{-10} , see also Figure 6.

The obtained approximation errors are plotted in Figure 3, which, for all the values of κ_\odot , shows linear convergence in the respective H^1 -norms for the error in u and u_\odot . Quadratic convergence can be seen for the multiplier in the norm of the intersection space $H^{-1/2}(\Lambda) \cap \kappa_\odot^{-1/2}H^{-1}(\Lambda)$. Without including the results we remark that the intersection norm is essential for obtaining robust approximation. In particular, we observed that measuring convergence in only the $H^{-1/2}$ -norm yields quadratic convergence for large values of κ_\odot while for small values the rate drops to linear.

Having verified the discretization scheme (and our implementation) we return to preconditioning and stability of the eigenvalue problem (9). We summarize the results in Figure 4 and Figure 5 which show the extrema, i.e. minimum and maximum absolute values, of the eigenvalues λ_h of the discretized problem (9). We note that the bounds are plotted together with

¹In all the presented numerical examples FEniCS[29]-based module FEniCSii[21] was used to discretize the coupled problems.

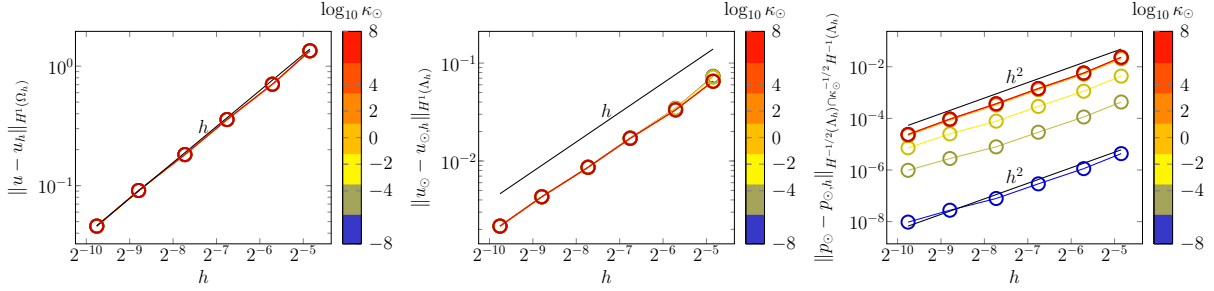


FIGURE 3. Approximation errors of \mathbb{P}_1 discretization of (7) for different values of κ_{\odot} .

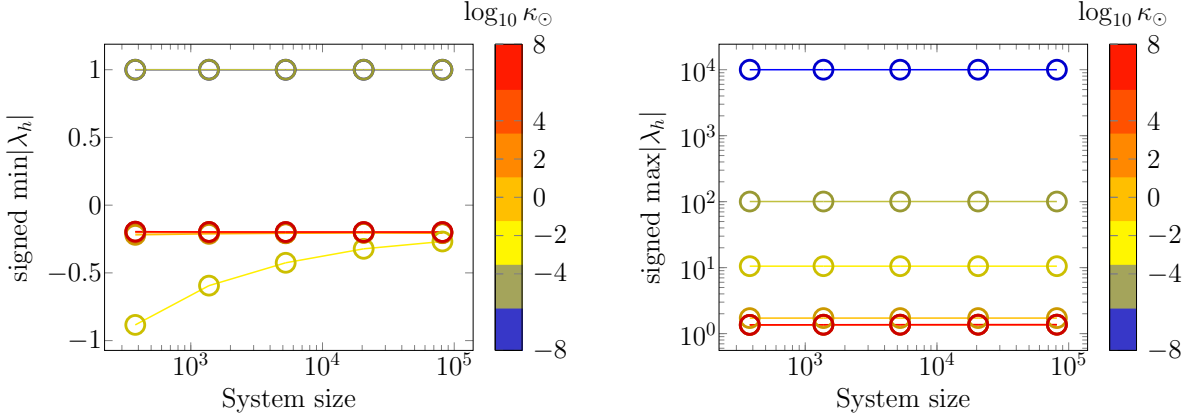


FIGURE 4. Performance of preconditioner \mathcal{B}_0 from (8) for problem (7) with varying κ_{\odot} . Here $\Omega = (-1, 1)^2$, Γ_{ε} is a circle of radius $\varepsilon = 0.1$. All the finite element spaces are discretized by \mathbb{P}_1 elements. The preconditioner does not yield κ_{\odot} -bounded condition numbers.

their sign which carries relevant information related e.g. to the discrete inf-sup or coercivity conditions.

Using \mathcal{B}_0 , the extremal eigenvalues of (9) are displayed in Figure 4. We observe that for each κ_{\odot} the quantities are bounded in h verifying stability of the discrete problem with \mathbb{P}_1 elements and the norm induced on Y by \mathcal{B}_0^{-1} , see [24]. However, there is an apparent growth of the largest in magnitude eigenvalue as κ_{\odot} becomes small. As such \mathcal{B}_0 does not yield parameter robust solver. On the other hand, the preconditioner \mathcal{B}_1 yields spectral bounds that are stable in κ_{\odot} and mesh refinement. We note that for small κ_{\odot} the observed upper and lower bounds are close to their theoretical values [31, 37] of $(1 + \sqrt{5})/2$ and $(1 - \sqrt{5})/2$ respectively. This is due to the multiplier norm being then dominated by the matrix of the H^{-1} -inner product such that the discrete preconditioner (which computes $-\Delta_{\Lambda}^{-1}$ by LU decomposition) is close to being the exact Schur complement preconditioner.

To illustrate how the conditioning translates to performance of iterative solvers Figure 6 reports the iteration counts of the MinRes solver using the two preconditioners (8). Here we reuse the setup of the previous eigenvalue experiments while the right hand side f in (7) is based on the manufactured solution setup described above. For each value of κ_{\odot} and the mesh size the solver is started from 0 initial guess and terminates once the preconditioned residual norm is reduced by factor 10^{10} . Both preconditioners are computed exactly using LU for the two leading blocks while the multiplier block, in particular the fractional term $-\Delta_{\Lambda}^{-1/2}$ is realized via spectral decomposition², see [24] for precise definition.

In Figure 6 it can be seen that for large values of κ_{\odot} both preconditioners yield iterations which are stable in mesh refinement. However, for small values, i.e. when the term $\kappa_{\odot}^{-1}\Delta_{\Lambda}^{-1}$

²Spectral decomposition is not suitable for practical applications because of its cubic scaling. However, Riesz maps in intersections of fractional order Sobolev spaces can be approximated with optimal complexity by rational approximations [5].

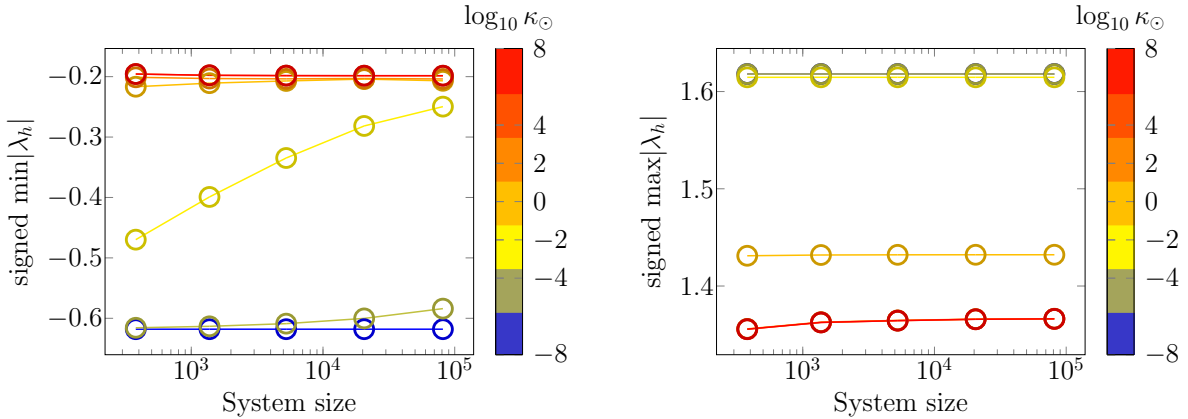


FIGURE 5. Performance of preconditioner \mathcal{B}_1 from (8) for 2d-1d coupled problem (7) with varying κ_{\odot} . Setup as in Figure 4. Preconditioner is robust in κ_{\odot} and mesh size.

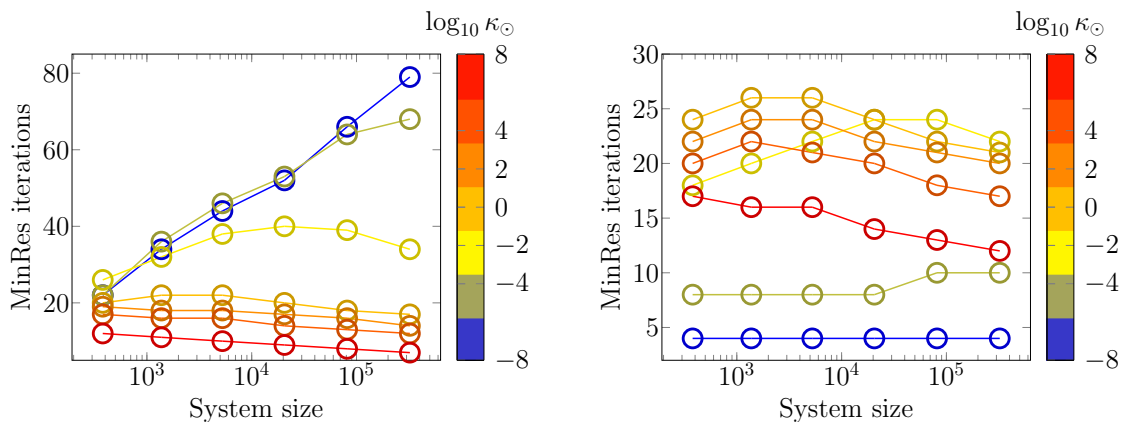


FIGURE 6. Convergence of (8)-preconditioned MinRes solver for problem (7) with varying κ_{\odot} . Only the preconditioner \mathcal{B}_1 (right) reflecting $p_{\odot} \in H^{-1/2} \cap \kappa_{\odot}^{-1/2} H^{-1}$ is parameter robust. Setup as in Figure 4.

becomes large, \mathcal{B}_0 shows dependence on the parameter. We conclude that the intersection space exploited in the definition of \mathcal{B}_1 is crucial for parameter robustness.

3. DEFINITION OF A PRECONDITIONER FOR THE 3d-1d PROBLEM: PERFORMANCES AND DRAWBACKS

At this point let us return to the original coupled 3d-1d problem (6) that we shall now consider with a preconditioner

$$\mathcal{B} = \begin{pmatrix} -\kappa\Delta & & \\ & -\kappa_{\odot}\varepsilon^2\Delta_{\Lambda} & \\ & & -\frac{\varepsilon^2}{\kappa}\Delta_{\Lambda}^{-1/2} - \kappa_{\odot}^{-1}\Delta_{\Lambda}^{-1} \end{pmatrix}^{-1}, \quad (11)$$

i.e. the Riesz operator associated to the inner product of the space in which well-posedness of (6) was shown in Theorem 2.1.

In order to test (11) we consider cylindrical domains Ω_{\oplus} , Ω_{\ominus} each with height 1 and radii of 0.5 and ε respectively. Following [22] we discretize $\Omega = \Omega_{\oplus} \cup \Omega_{\ominus}$ such that the mesh conforms both to the interface Γ_{ε} and the centerline Λ , see Figure 7. We remark that the conformity assumption was used in [22] to show stability of the discrete problem with \mathbb{P}_1 elements (used below). At the same time, the assumption leads to greatly refined meshes in the vicinity of Γ_{ε} . It also increases the cost of mesh generation and, due to the size of the resulting system,

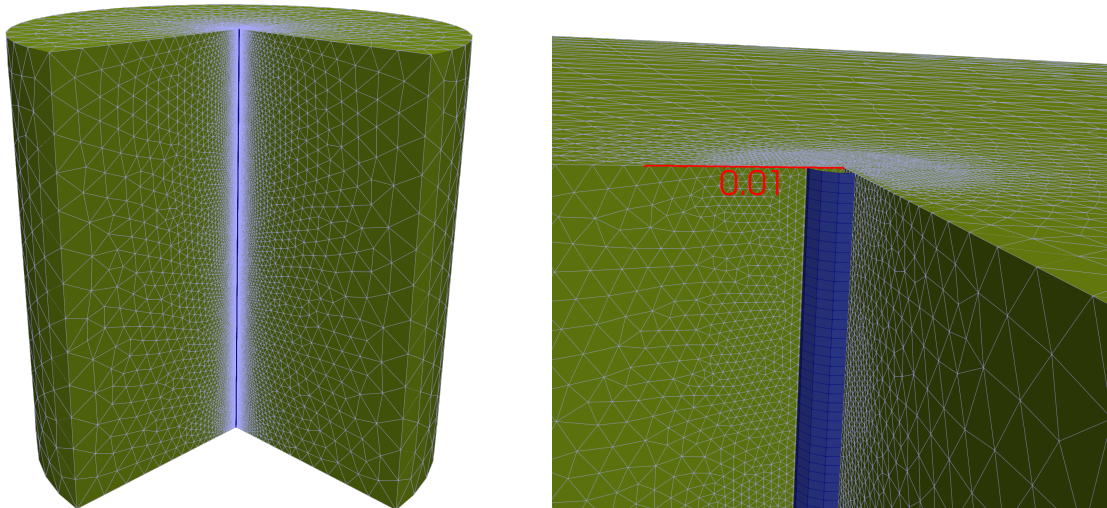


FIGURE 7. Computational mesh considered in experiments for the coupled $3d-1d$ problem (11). Here $\varepsilon = 2 \cdot 10^{-3}$. Mesh of Ω conforms to the centerline Λ as well as to the coupling surface Γ_ε leading to high refinement near Λ (edges of the mesh elements are pictured in light blue color). (Right) Virtual surface used for computing $\overline{\mathcal{T}}_\Lambda$ is rendered in dark blue color.

restricts³ the type of experiments we can perform (on our serial computational setup). In the following we shall thus limit the computational study only to robustness of iterative methods. We remark that stable discretization of (11) is possible also if the mesh of Ω is independent of Λ and Γ , cf. [22]. However, we argue that the conforming setup is simpler and more transparent.

In Figure 8 we report on the convergence of the MinRes solver using preconditioner (11) for $2 \cdot 10^{-3} \leq \varepsilon \leq 10^{-1}$ and two parameter regimes. Here the action of the leading block $-\kappa\Delta^{-1}$ of (11) is approximated in terms of (i) a single V-cycle of algebraic multigrid (AMG) and (ii) 10 steps of preconditioned conjugate gradient (PCG) method using AMG as preconditioner. The remaining two blocks of (11) are computed by LU factorization. We remark that the choice (i) is more practical while with (ii) the preconditioner is almost exact as the absolute residual norm after the 10 PCG steps is typically $< 10^{-15}$ in our case. With (ii) we thus aim to ensure that the effects of parameter variations on MinRes convergence are (mostly) due to the construction of the multiplier preconditioner. In both cases the convergence criterion for the MinRes solver requires reducing the preconditioned residual norm by a factor 10^{10} . Finally, the coupling operator $\overline{\mathcal{T}}_\Lambda$ is approximated using a Legendre quadrature of degree 20.

Considering the results in Figure 8 we observe that performance of the preconditioner differs dramatically between the two regimes. When $\kappa = 10^8$, $\kappa_\odot = 10^{-8}$, such that the H^{-1} -term can dominate the multiplier block in \mathcal{B} , the iteration counts are practically independent of ε . Note that here only the construction (i) for the leading block is considered as it already yields low enough iterations. On the other hand, with $\kappa = 10^{-8}$, $\kappa_\odot = 10^8$ the solver performance deteriorates for small radii. This is true for the construction (i) which, for the different radii $\varepsilon \in \{1 \cdot 10^{-1}, 5 \cdot 10^{-2}, 1 \cdot 10^{-2}, 5 \cdot 10^{-3}, 2 \cdot 10^{-3}\}$ and the finest refinement levels yields the iterations counts of 37, 44, 58, 71, 100 as well as for (ii) where convergence is reached respectively after 28, 31, 40, 46, 68 iterations.

The unbounded iterations, in particular with preconditioner (ii), bring into question the stability of the coupled $3d-1d$ problem (6) with preconditioner (11) and in particular the intersection space Q_\odot for the multiplier. The lack of robustness is surprising as it suggests that radius ε in (6) does not behave as a standard material parameter in the sense that corresponding weighting in the (appropriate) intersection space does not yield robustness with respect to its variations.

³As an example, for radius $\varepsilon = 1 \cdot 10^{-2}$ the finest mesh considered contained roughly 11 million tetrahedra. Using \mathbb{P}_1 elements the number of $3d$ unknowns is then ~ 2 million while the multiplier space has ~ 2 thousand degrees of freedom.

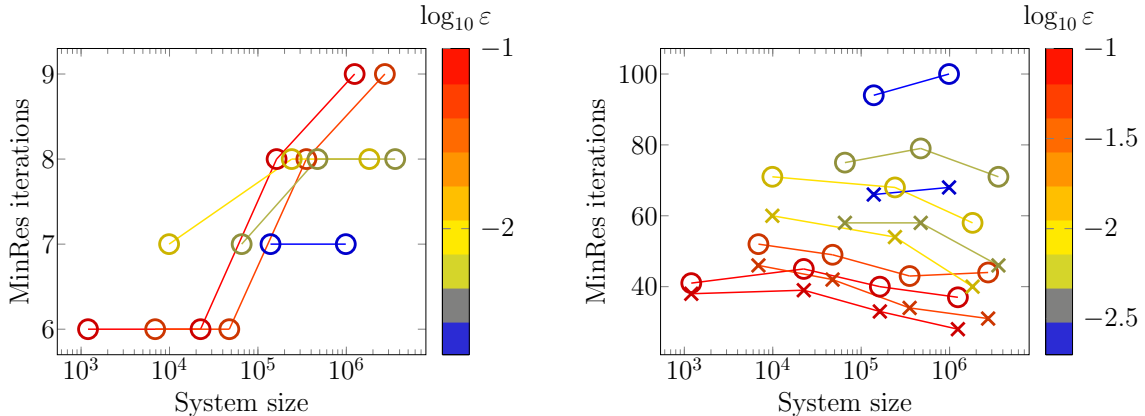


FIGURE 8. Performance of preconditioner (11) for the coupled 3d-1d problem (6) and varying radius. (Left) We set $\kappa = 10^8$, $\kappa_\circ = 10^{-8}$. (Right) We set $\kappa = 10^{-8}$, $\kappa_\circ = 10^8$. The leading block of the preconditioner uses single AMG V-cycle (\circ markers) or 10 PCG iterations with AMG preconditioner (\times markers). The remaining blocks are realized by LU.

However, this result may be qualitatively justified on the basis of the stability analysis, where we noticed the influence of the constant C_{IT} in the inf-sup condition. We will show in the next section that C_{IT} may depend on ε , which may explain the findings in Figure 8.

Varying radius in 2d-1d preconditioning example. In order to gain more insight into the observation that in the 3d-1d setting of (6) the multiplier preconditioner reflecting the intersection space $\kappa^{-1/2}\varepsilon H^{-1/2} \cap \kappa_\circ^{-1/2} H^{-1}$ did not lead to robustness, let us return to the 2d-1d operator (7). Next, we shall investigate the properties of the preconditioner \mathcal{B}_1 when ε varies. We recall that \mathcal{B}_1 was found to be robust with respect to the material parameters.

Using the previous experimental setup, Figure 9 shows the performance of the preconditioner when $\kappa_\circ = 10^{10}$ and $\varepsilon \leq 10^{-1}$. Here, by the choice of a large κ_\circ we wish to put emphasis on the fractional part of the multiplier preconditioner, which, analogously to Theorem 2.1, brings the inverse trace constant into the Brezzi estimates. In Figure 9 we observe that while the largest eigenvalues are bounded in ε , the smallest in magnitude eigenvalue approaches 0 as Λ_ε shrinks. We note that for all ε the two eigenvalue bounds are stable in mesh size h . In the figure we further report convergence history of the MinRes solver (run with the same settings as in the previous experiments). We observe that for small radii the iteration counts grow rapidly with initial mesh refinement before decreasing back on finest meshes, cf. bounded iterations with mesh refinement in Figure 6. However, the limit $\varepsilon \rightarrow 0$ does not seem to affect the iterative solver as clearly as the blow up of the condition number, cf. $\min|\lambda_h|$ in Figure 9. We attribute this behaviour to the specific choice of the right-hand side and 0 initial guess in our numerical setup. Nevertheless, the sensitivity to the radius furthers our claim of the special role of ε in understanding preconditioner robustness.

4. THE ROLE OF THE INNER RADIUS ON MIXED-DIMENSIONAL PROBLEMS

As discussed in the preceding sections, it has been observed that the robustness of the preconditioner (11) diminishes as the inner radius of the inclusion approaches zero. This behavior is not limited to the 3d-1d preconditioner formulation but is also evident in the 2d-1d examples. Consequently, it suggests that the detrimental effect of ε is not a result of the dimensional reduction technique itself but rather inherent in the mathematical structure of the problem.

Specifically, the dependence on ε is manifested in the constant of the inf-sup stability property. The analysis in Theorem 2.1 reveals that the boundedness constant C_B of the bilinear form b remains independent of the inner diameter. However, the inf-sup constant β is not guaranteed to be independent of ε as the presence of the inverse trace constant C_{IT} introduces questions regarding its independence from the inner radius. The inverse trace theorem, a well-established

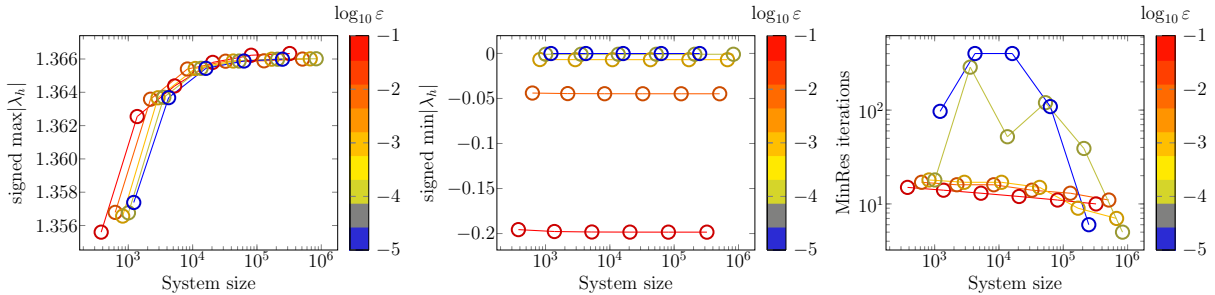


FIGURE 9. Performance of preconditioner \mathcal{B}_1 in (8) for problem (7) with $\kappa_{\odot} = 10^{10}$, $\Omega = (-1, 1)^2$, Γ_{ε} is a circle of radius $10^{-5} \leq \varepsilon \leq 10^{-1}$. All the finite element spaces are discretized by \mathbb{P}_1 elements. (Left, center) The conditioning deteriorates with ε as the largest in magnitude eigenvalue (9) is bounded in the parameter while the smallest in magnitude eigenvalue decreases with ε . (Right) For small radii the iterations are not stable (maximum number of allowed iterations is set to 400).

result in functional analysis, provides insights into this matter (see, for example, [40], [32], [28]). However, deriving an accurate bound for C_{IT} is a challenging task, particularly when considering a parameterized domain.

In this section, our objective is to investigate the relationship between the inf-sup constant β and the parameter ε , which is closely associated with the inverse trace constant C_{IT} . To accomplish this, we analyze a simplified yet significant scenario that allows us to elucidate the connection between the inf-sup constant and the inner radius.

4.1. The 2d-1d formulation for the perforated domain problem. Let us consider a generalized cylindrical vessel immersed in a three-dimensional domain Ω . The vessel surface is denoted by Γ_{ε} , where ε indicates the cylinder radius. We are interested in studying how the mathematical structure of the problem behaves when $\varepsilon \rightarrow 0$. A straightforward approach can be to select a slice of Ω , here denoted by the superscript “*”, such that we obtain a domain Ω^* ,

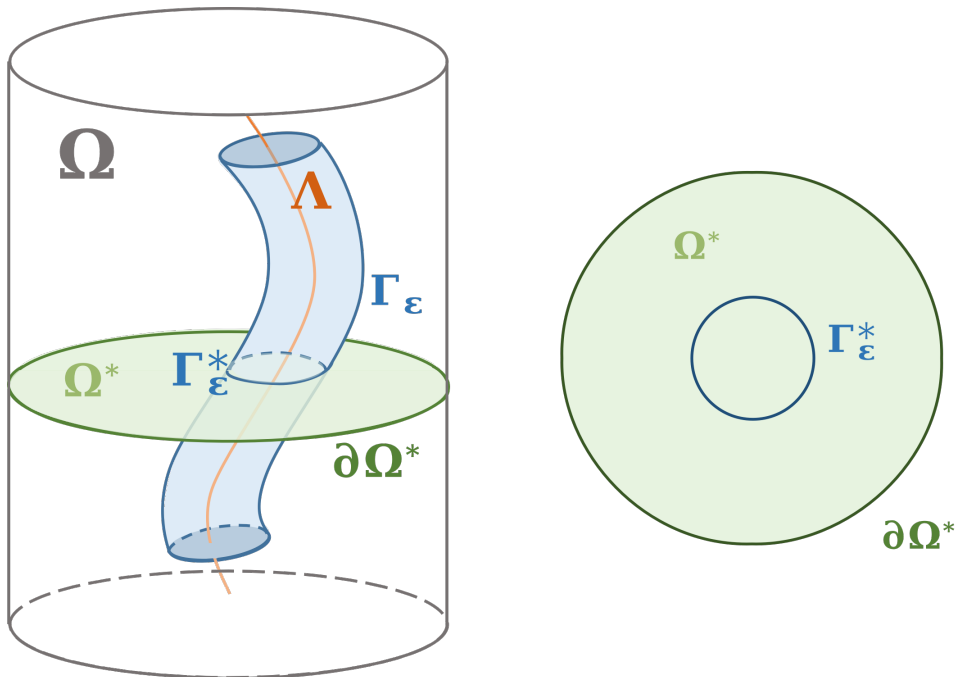


FIGURE 10. (Left) Pictorial representation of a vessel with radius ε , centerline Λ and boundary Γ_{ε} immersed in a three-dimensional domain Ω . By cutting a slice of Ω , we obtain the two-dimensional domain Ω^* with boundary $\partial\Omega^*$ and circular one-dimensional inclusion Γ_{ε}^* . (Right) Pictorial representation of the slice-domain Ω^* .

where the curve Γ_ε^* is the restriction of Γ_ε on the slice, see Figure 10. Clearly, $\text{diam}\Gamma_\varepsilon^*$ depends on ε . In turn, studying the effects of shrinking $\text{diam}\Gamma_\varepsilon^*$ in Ω^* (a 2d-1d system) is representative of the effects of the diminishing vessel/inner radius. The underlying assumption is the complete decoupling of the radius influence from the axial direction, which seems reasonable when considering cylindrical setting. Indeed, inspecting the expression of the Laplacian in cylindrical coordinates

$$\Delta = \frac{1}{\rho} \frac{\partial}{\partial \rho} \left(\rho \frac{\partial}{\partial \rho} \right) + \frac{1}{\rho^2} \frac{\partial^2}{\partial \phi^2} + \frac{\partial^2}{\partial z^2}$$

corroborates the assumption: ρ (and in turn ε) does not appear in the axial derivative part. From now, until the end of this section, the superscript "*" will be omitted, so that Ω and $\partial\Omega$ will refer respectively to the 2d sliced domain and its outer boundary. Moreover, Γ_ε will denote the one-dimensional closed curve embedded in Ω^* .

Let us consider the following ε -dependent Poisson problem defined on Ω :

$$\begin{aligned} -\Delta u &= 0 & \text{on } \Omega, \\ u|_{\Gamma_\varepsilon} &= g & \text{on } \Gamma_\varepsilon, \\ u &= 0 & \text{on } \partial\Omega, \end{aligned} \tag{12}$$

where $\Gamma_\varepsilon \cap \partial\Omega = \emptyset$ and u is a two-dimensional scalar field defined on Ω . Now consider a mixed weak formulation of (12), where the boundary condition on Γ_ε is enforced weakly by a Lagrange multiplier in order for the the mathematical structure of (12) to mirror the 3d-1d problem. The variational problem reads:

$$\begin{aligned} (\nabla u, \nabla v)_\Omega + (p_\odot, \mathcal{T}v)_{\Gamma_\varepsilon} &= 0 & \forall u, v \in H_0^1(\Omega) \\ (\mathcal{T}u, q_\odot)_{\Gamma_\varepsilon} &= (g, q_\odot)_{\Gamma_\varepsilon} & \forall p_\odot, q_\odot \in H^{-1/2}(\Gamma_\varepsilon) \end{aligned} \tag{13}$$

Note that the solution operator \mathcal{A} of (13) has the following block structure

$$\mathcal{A} = \begin{pmatrix} A & B' \\ B & 0 \end{pmatrix}, \quad \langle Au, v \rangle_\Omega = \int_\Omega \nabla u \cdot \nabla v, \quad \langle Bu, q_\odot \rangle_{\Gamma_\varepsilon} = \int_{\Gamma_\varepsilon} p_\odot v.$$

The question we address next is that of well-posedness of the variational formulation (13) when $\varepsilon \rightarrow 0$. In the framework of saddle-point problems, the boundedness of the bilinear forms a, b in case of (13) can be easily established with the respective constants equal to 1. Regarding the existence of the Brezzi inf-sup constant β , a straightforward proof will make use of the following theorem [40]:

Theorem 4.1. (Inverse Trace Theorem) *Given the necessary smoothness assumption for Ω , the trace operator $\mathcal{T} : H^1(\Omega) \rightarrow H^{1/2}(\Gamma_\varepsilon)$ has a continuous right inverse operator*

$$\mathcal{E} : H^{1/2}(\Gamma_\varepsilon) \rightarrow H^1(\Omega)$$

satisfying $\mathcal{T}\mathcal{E}w_\odot = w_\odot$ for all $w_\odot \in H^{1/2}(\Gamma_\varepsilon)$ as well as

$$\|\mathcal{E}w_\odot\|_{H^1(\Omega)} \leq C_{IT} \|w_\odot\|_{H^{1/2}(\Gamma_\varepsilon)} \quad \forall w_\odot \in H^{1/2}(\Gamma_\varepsilon).$$

Then, by taking $v = \mathcal{E}v_{q_\odot}$, where, by v_{q_\odot} , we intend an element of $H^{1/2}(\Gamma_\varepsilon)$ such that the following Riesz mapping properties hold

$$\langle v_{q_\odot}, w_\odot \rangle_{H^{1/2}(\Gamma_\varepsilon)} = (q_\odot, w_\odot)_{\Gamma_\varepsilon} \quad \text{and} \quad \|v_{q_\odot}\|_{H^{1/2}(\Gamma_\varepsilon)} = \|q_\odot\|_{H^{-1/2}(\Gamma_\varepsilon)},$$

we obtain that

$$\sup_{v \in H_0^1(\Omega), v \neq 0} \frac{(\mathcal{T}v, q_\odot)_{\Gamma_\varepsilon}}{\|v\|_{H_0^1(\Omega)}} \geq \frac{(v_{q_\odot}, q_\odot)_{\Gamma_\varepsilon}}{\|\mathcal{E}v_{q_\odot}\|_{H_0^1(\Omega)}} = \frac{\langle v_{q_\odot}, v_{q_\odot} \rangle_{H^{1/2}(\Gamma_\varepsilon)}}{\|\mathcal{E}v_{q_\odot}\|_{H_0^1(\Omega)}} \geq \frac{1}{C_{IT}} \|v_{q_\odot}\|_{H^{1/2}(\Gamma_\varepsilon)}.$$

What is apparent from the above calculation, is, again, the structural relationship between the existence of the inf-sup constant β , and the inverse trace inequality constant C_{IT} i.e $\beta = 1/C_{IT}$. This suggests (and it is what we want to uncover) a tight relationship between β and the inner radius by means of the *trace inequality constant* C_T . Indeed from Lemma 2.2 in [19], the ε influence is made clear:

Lemma 4.1 (Lemma 2.2 in [19]). *Let $B_\varepsilon \subset \mathbb{R}^2$ be a circle with a sufficiently small radius ε and $v \in H_0^1(\Omega)$. Then we have:*

$$\|\mathcal{T}v\|_{L^2(\partial B_\varepsilon)} \leq C_T \|v\|_{H_0^1(\Omega)} = C\sqrt{\varepsilon|\log \varepsilon|} \|v\|_{H_0^1(\Omega)} \quad (14)$$

with C positive and independent of ε .

By considering that the extension operator, \mathcal{E} , is the right inverse of the trace, \mathcal{T} , the following claim is proposed: *the vessel radius ε directly affects the inf-sup constant β through the trace inequality constant C_T* . This claim sounds reasonable if one considers that β directly characterizes the lower bound of the bilinear form b , which depends strongly on the trace operator; moreover, it is corroborated by the fact that $\beta = 1/C_{IT}$ so that, assuming a relation between the trace inequality and the inverse trace one, we get that ε directly affects β . That said, in order to prove the claim, it would be required to track in detail the exact expression for C_{IT} , obtaining, thus, a direct link between β and ε . Establishing such an analytical expression for C_{IT} can be a very intricate task, especially when the domain size needs to be considered as the parameter. Nonetheless, we can rely on numerical analysis and employ the computability of the constants in a discretized setting, as follows.

Brezzi inf-sup constant evaluation. Let $V = H_0^1(\Omega)$, $Q = H^{-1/2}(\Gamma_\varepsilon)$ and $\|\cdot\|_V$ be the H_0^1 -norm (induced by the operator A) while $\|\cdot\|_Q$ shall be the $H_\Gamma^{-1/2}$ -norm induced by the fractional operator $N := (-\Delta + I)^{-1/2}$ (where both the terms are understood to be defined on Γ_ε). Consider now a family (V_h, Q_h) of discretization of (V, Q) characterized by the following discrete Brezzi inf-sup constant

$$\sup_{v \in V_h, v \neq 0} \frac{b(v, q_\circ)}{\|v\|_{V_h}} \geq \beta_h \|q_\circ\|_{Q_h} \quad \forall q_\circ \in Q_h. \quad (15)$$

If (V_h, Q_h) is a *stable* discretization i.e. both the discrete Brezzi inf-sup and coercivity constants are bounded from below by a constant which is independent from h [1], [36]:

$$\{\beta_h\}_{h \rightarrow 0} \geq \beta > 0, \quad (16)$$

then an approximation of β can be obtained by considering the truncated limit $\{\beta_h\}_{h \rightarrow \delta}$, for δ sufficiently small. With the purpose of computing β_h , we recall the following lemma by Qin [35]:

Lemma 4.2 (Qin [35]). *Given a stable discretization (V_h, Q_h) for the saddle point problem (13), consider the following generalized eigenproblem: Find $\lambda \in \mathbb{R}$, $0 \neq (u, p_\circ) \in V_h \times Q_h$ such that*

$$\langle u_h, v \rangle_V + b(v, p_\circ) + b(u_h, q_\circ) = -\lambda \langle p_\circ, q_\circ \rangle_Q \quad \forall (v, q_\circ) \in V_h \times Q_h. \quad (17)$$

Then, $\lambda \geq 0$ and $\beta \approx \beta_h = \sqrt{\lambda^{\min}}$.

In the framework of problem (13), the eigenproblem can be recasted in the following form involving the Schur complement of \mathcal{A} : Find $p_\circ \in Q_h$, $\lambda_B > 0$ such that⁴

$$BA^{-1}B'p_\circ = \lambda_B^2 Np_\circ \quad \text{in } Q'_h. \quad (18)$$

Here the subscript B , which stands for ‘‘Brezzi’’, has been introduced for clarity of notation as will become clear soon. In particular, for stability of the discrete problem (13), $\lambda_B^{\min} = \min \lambda_B$, $\lambda_B^{\max} = \max \lambda_B$ shall be independent from the mesh size h . We remark that in this framework $\lambda_B^{\min} \approx \beta$.

⁴Though it is λ_B^2 that is the eigenvalue of (18) we shall in the following, with a slight abuse of notation, refer to $\max \lambda_B = \lambda_B^{\max}$, $\min \lambda_B = \lambda_B^{\min}$ as the eigenvalue bounds, extremal eigenvalues or simply eigenvalues. This choice is intended to simplify notation and avoid proliferation of $\sqrt{\cdot}$ in the text. Similar convention will be applied also with the Steklov eigenvalue problems (19) and (23).

Trace constant evaluation. Let us consider the eigenvalue problem defined on the domain in Figure 10, which reads as follows:

$$\begin{aligned} -\Delta u &= 0 && \text{in } \Omega \subset \mathbb{R}^2, \\ \nabla u \cdot \nu &= \lambda_S^{-2} u && \text{on } \Gamma_\varepsilon, \\ u &= 0 && \text{on } \partial\Omega, \end{aligned} \quad (19)$$

where ν is the unit normal to Γ_ε . We remark that (19) is a variant of the Steklov eigenvalue problem. For rigorous mathematical treatment of (19) we refer to e.g. [15] and references therein.

The weak formulation of (19), leads to the generalized eigenproblem: Find $u \in H_0^1(\Omega)$, $\lambda_S > 0$ satisfying

$$\int_{\Gamma_\varepsilon} uv = \lambda_S^2 \int_{\Omega} \nabla u \cdot \nabla v \quad \forall v \in H_0^1 \quad (20)$$

so that, λ_S^{\max} allows for estimates of the $L^2(\Gamma_\varepsilon)$ -norm of u in terms of the $H_0^1(\Omega)$ -norm. Indeed, we have $\|u\|_{L^2(\Gamma_\varepsilon)} \leq \lambda_S^{\max} \|u\|_{H_0^1(\Omega)}$ for all $u \in H_0^1(\Omega)$.

Once the eigenproblems (17), (19) are properly discretized (from now on subscript h will denote the discretized analogues of a given quantity; subscript ε_i will denote a quantity evaluated on a domain with inner/inclusion radius equal to ε_i), the numerical tools for the evaluation of the inf-sup constant β and the trace inequality constant C_T are readily established. We can, thus, proceed with the investigation of the influence of ε in the considered mathematical framework.

The research path is summarized in Figure 11. Due to the analytical difficulty in the evaluation of the role of the inner radius in the inverse trace constant C_{IT} , and its relationship with the trace constant, we shift our inquiry to a discretized setting, by dint of the discretized eigenproblems. What will be done is a concomitant evaluation of $\{\beta_{h,\varepsilon_i}\}_{\varepsilon_i \in I}$ and $\{C_{T_{h,\varepsilon_i}}\}_{\varepsilon_i \in I}$, where $I = \{\varepsilon_0, \varepsilon_1, \dots, \varepsilon_n\}$ and $\varepsilon_0 > \varepsilon_1 > \dots > \varepsilon_n$ with $\varepsilon_n \ll 1$. Then, if some noticeable correlation between λ_B^{\min} and λ_S^{\max} exists, then it also holds for $\{\beta_{h,\varepsilon_i}\}$ and $\{C_{T_{h,\varepsilon_i}}\}$ (by means of (17), (18)) so that we can find numerical evidence to support our claim.

4.2. Numerical results about the 2d-1d formulation. Here we summarize the numerical experiments concerning the evaluation of $\{\beta_{h,\varepsilon_i}\}$ and $\{C_{T_{h,\varepsilon_i}}\}$ with varying $\varepsilon_i \in I = \{10^{-1}, \dots, 10^{-5}\}$. For simplicity we shall at first limit the investigations to $\Omega = \{x \in \mathbb{R}^2, |x| < 1\}$, a circular inclusion $\Gamma_\varepsilon = \{x \in \Omega, |x| = \varepsilon\}$ and \mathbb{P}_1 discretization.

In Figure 12 we demonstrate that our choice of norms and finite element spaces yields a stable problem. More precisely, we observe that both the upper and lower bound on the Schur complement spectra are stable in mesh refinement for each ε fixed. Moreover, λ_B^{\max} appears to be bounded in the radius of Γ_ε , cf. Theorem 2.1. On the other hand, λ_B^{\min} seems to decrease together with ε .

We now propose that λ_B^{\min} is closely related to the Steklov eigenvalue problem (20). To investigate the relation between λ_S^{\max} and λ_B^{\min} , Figure 13 plots the relative error between the two quantities⁵ for varying values of ε . With the relative error $\sim 10^{-4}$ it appears that $\lambda_S^{\max} = \lambda_B^{\min}$. In Figure 13 we finally plot the dependence of λ_S^{\max} , λ_B^{\min} on the radius of Γ_ε . The observed dependence agrees well with the theoretical bound [19].

In order to corroborate the independence of the established relation between λ_B^{\min} and λ_S^{\max} from geometrical factors, we carry out the above analysis for a square-shaped inclusion, i.e. $\Gamma_\varepsilon = \partial(-\varepsilon, \varepsilon)^2$ in a squared domain $\Omega = (-1, 1)^2$. A comparison between the obtained values of $\lambda_S^{\max}(\varepsilon)$ and $\lambda_B^{\min}(\varepsilon)$, is depicted in Figure 14 (see also Appendix for additional results). No significant difference is reported. The relative error between the eigenvalues remains well below the percentage point and the expression $C\sqrt{\varepsilon|\log \varepsilon|}$ retraces $\lambda_B^{\min}(\varepsilon)$ with a constant $C \approx 1.116$.

Having shown independence of our observations from the shape of the inclusion/coupling surface, the effect of meshing strategy and finite element discretization will be investigated using a circular embedded domain Γ_ε . To exclude any relevant mesh influence on the obtained

⁵For each ε we consider a sequence of eigenvalues λ_{h_l} computed on meshes with sizes h_l . We terminate the sequence once the relative error between subsequent eigenvalues, $|\lambda_{h_l} - \lambda_{h_{l+1}}|/\lambda_{h_l}$, is less than 10^{-4} .

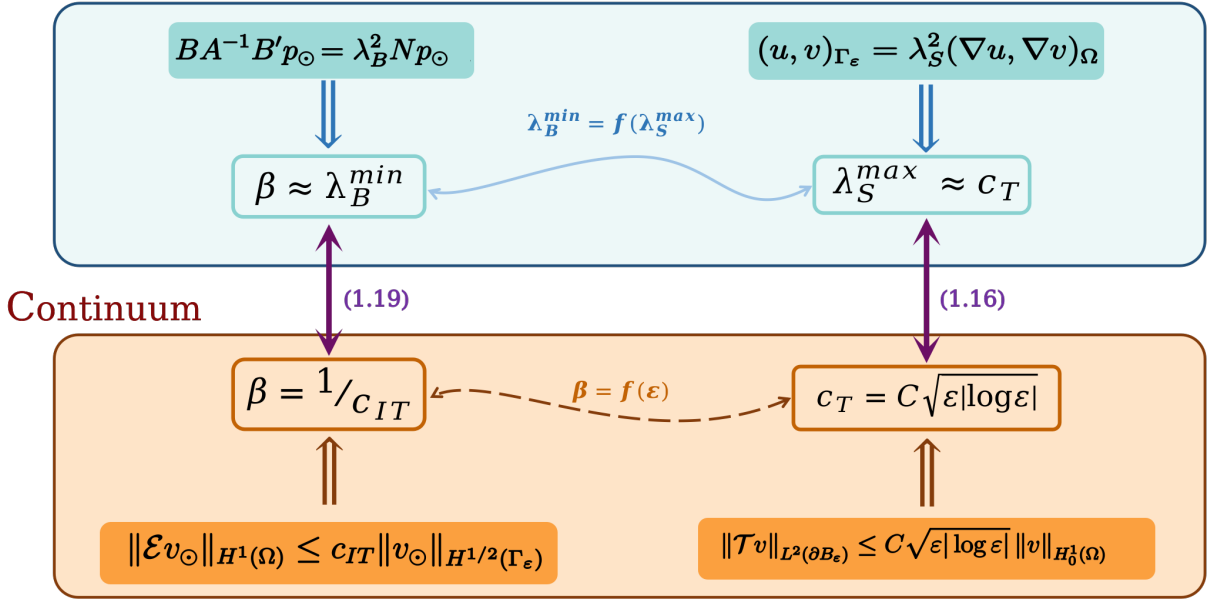
\mathbb{P}^1 discretization

FIGURE 11. Pictorial representation of the path followed in the analysis of the role of ε on β . Thanks to the evaluation of the eigenvalues of problems (18) and (19), a relation can be established between λ_B^{\min} and λ_S^{\max} . Then, by virtue of equations (14) (20) (represented by the purple arrows) bridging the discrete setting to the continuous one, we can close the loop and determine a relation between the Brezzi inf-sup constant β and the inner radius ε .

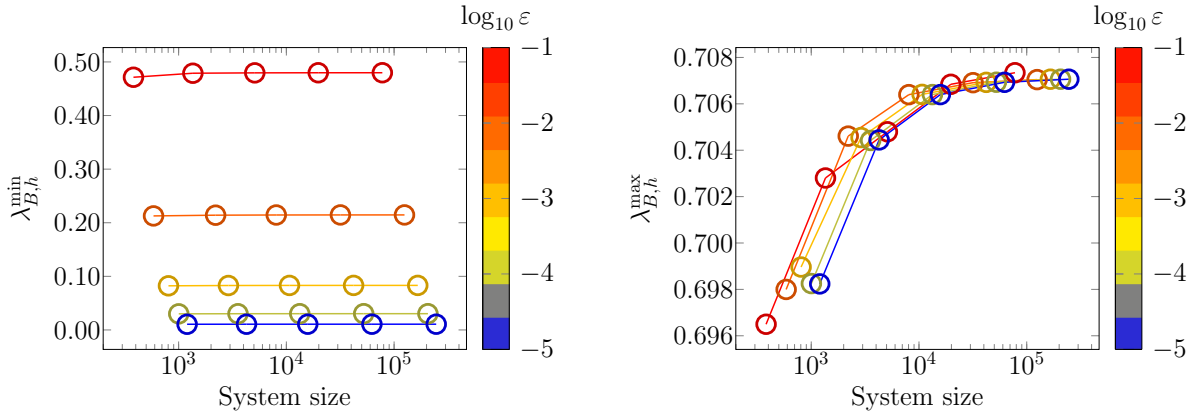


FIGURE 12. (Left) Mesh convergence of the extremal eigenvalues of Schur complement (18) for $\Omega = \{x \in \mathbb{R}^2, |x| < 1\}$, $\Gamma_{\varepsilon} = \{x \in \Omega, |x| = \varepsilon\}$. Both spaces V and Q are discretized by \mathbb{P}_1 elements. For each ε a sequence of problems is considered on uniformly refined meshes starting from size $h_0 \geq h_l \geq h_{\min}$ leading to eigenvalues λ_{B,h_l} .

results, the same analysis has been repeated on a specific type of mesh, which we shall refer to as *layered*, and which has the peculiarity of being Γ_{ε_i} -conformal (Ω vertices and edges match with Γ_{ε_i} ones) for every value of $\varepsilon_i \in I$ simultaneously, cf. Figure 15. In such a way, the mesh configuration, which is the same for every value of the inner radius, cannot be held responsible for any effects on λ - ε relations. The results are plotted in Figure 16 (left). The relative difference between the values of $\lambda_B^{\max}(\varepsilon)$, $\lambda_B^{\min}(\varepsilon)$ and $\lambda_S^{\max}(\varepsilon)$ obtained on different meshes (each conformal to a specific Γ_{ε_i}) and the ones obtained on the layered mesh differs by less than one percentage point. Accordingly, the same relation plotted in Figure 13 between $\lambda_S^{\max}(\varepsilon)$ and $\lambda_B^{\min}(\varepsilon)$ holds also for the values obtained on the layered mesh. In conclusion the results do not undergo

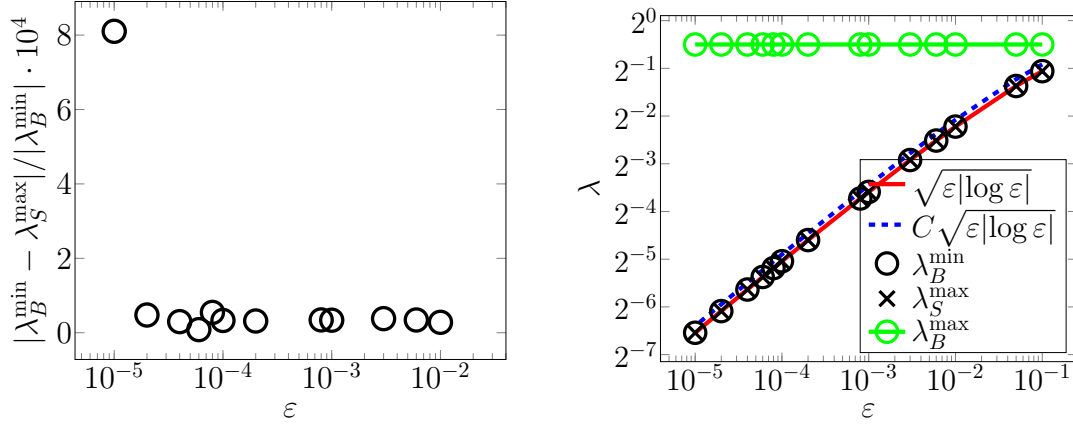


FIGURE 13. (Left) Error between the smallest eigenvalue λ_B^{\min} of the Schur complement problem (18) and the largest eigenvalue λ_S^{\max} of the Steklov problem (20). In both cases, values from the finest level of refinement are considered, i.e. $\lambda_X := \lambda_{X,h_{\min}}$. (Right) Dependence of the Schur complement eigenvalues on the radius of coupling curve $\Gamma_\varepsilon = \{x \in \Omega, |x| = \varepsilon\}$. Value $C \approx 0.999$ is obtained by fitting values λ_B^{\min} for $\varepsilon < 10^{-1}$.

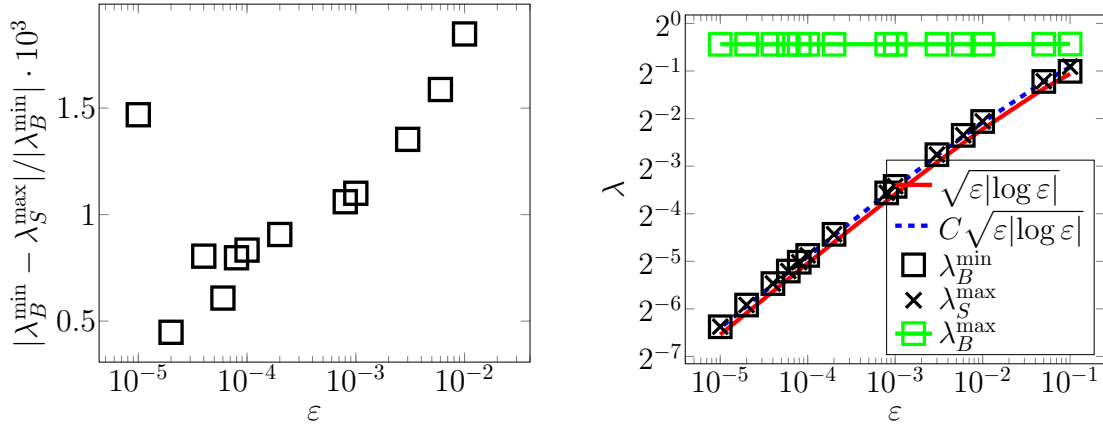


FIGURE 14. (Left) Error between the smallest eigenvalue λ_B^{\min} of the Schur complement problem (18) and the largest eigenvalue λ_S^{\max} of the Steklov problem (20) on squared domain $\Omega = (-1, 1)^2$. In both cases, values from the finest level of refinement are considered, i.e. $\lambda_X := \lambda_{X,h_{\min}}$. (Right) Dependence of the Schur complement eigenvalues on the radius of coupling curve $\Gamma_\varepsilon = \partial(-\varepsilon, \varepsilon)^2$. Value $C \approx 1.116$ is obtained by fitting values λ_B^{\min} for $\varepsilon < 10^{-1}$.

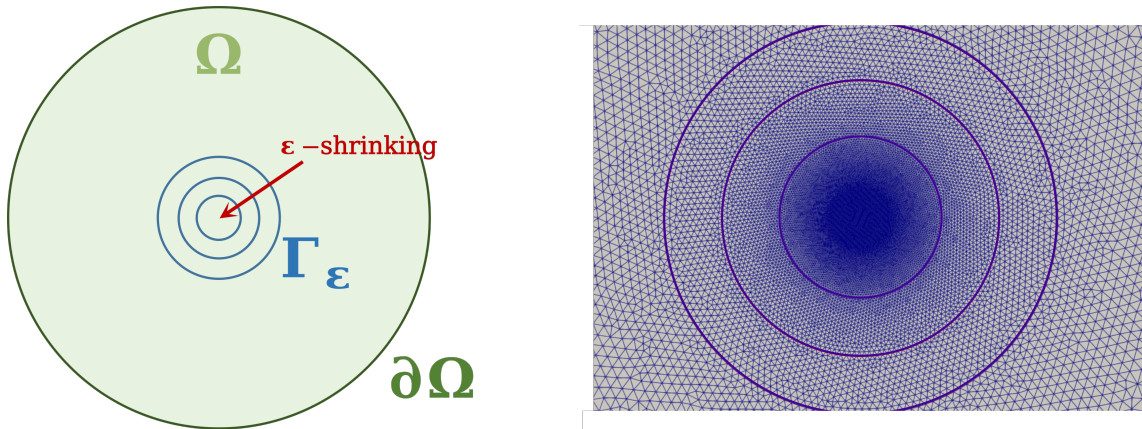


FIGURE 15. (Left) Pictorial representation of the inner-radius shrinking process. (Right) Partial representation (zoomed toward the Ω center) of the *layered* mesh. The mesh has the property of being conforming simultaneously to every Γ_{ε_i} , $\varepsilon_i \in I$ (purple circles).

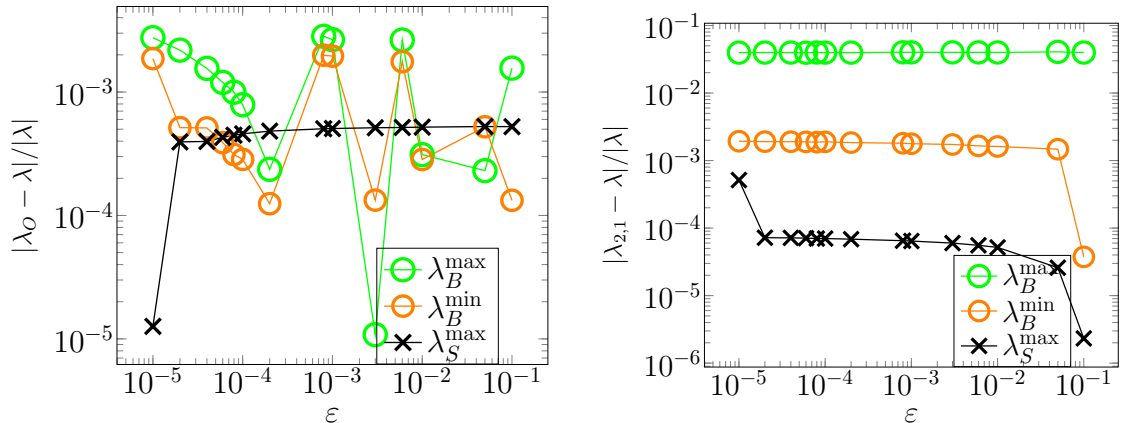


FIGURE 16. Relative error $|\lambda_* - \lambda|/|\lambda|$, where λ spans $\{\lambda_B^{\max}, \lambda_B^{\min}, \lambda_S^{\max}\}$ eigenvalues obtained with standard meshing procedure (each grid conforming to a specific Γ_{ε_i} ; see Figure 13). (Left) $\lambda_* \equiv \lambda_O$ spans $\{\lambda_{B,O}^{\max}, \lambda_{B,O}^{\min}, \lambda_{S,O}^{\max}\}$ obtained on the *layered* mesh in Figure 15 and denoted by the subscript "O". (right) $\lambda_* \equiv \lambda_{2,1}$ spans $\{\lambda_{B,2,1}^{\max}, \lambda_{B,2,1}^{\min}, \lambda_{S,2,1}^{\max}\}$ obtained with a $\mathbb{P}_2 - \mathbb{P}_1$ discretization and denoted by subscript "2,1".

significant grid influence. Additional numerical results in support of this conclusion can be found in Appendix.

In addition to the geometrical (shape, mesh) factors, our aim is to exclude possible effects of different polynomial order between the $2d$ and $1d$ spaces. The results of the comparison between $\mathbb{P}_1 - \mathbb{P}_1$ and $\mathbb{P}_2 - \mathbb{P}_1$ discretization (continuous \mathbb{P}_2 elements for Ω and \mathbb{P}_1 elements for Γ_{ε_i}) are plotted in Figure 16. No noticeable difference can be attributed to the change of polynomial order, except for effects on $\lambda_B^{\max}(\varepsilon)$, which differ more than 1%, but still remain independent from ε_i . From this, we can deduce that also for the $\mathbb{P}_2 - \mathbb{P}_1$ discretization, $\lambda_B^{\min} \approx \lambda_S^{\max} \sim \sqrt{|\varepsilon| \log |\varepsilon|}$. Thus no relevant role of the polynomial degree on the results can be experienced (for detailed results see Appendix).

4.3. The $2d$ - $0d$ formulation for the perforated domain problem. The link between stability of (12) and inner radius ε via the constant of the inverse trace inequality, which we demonstrated above for $2d$ - $1d$ trace problem, naturally extends to $3d$ - $2d$ coupling as well. In connection with the $3d$ - $1d$ problem (3) we may then ask if the dimensional reduction removes to observed affect of ε . To address this question we continue our investigations by applying model reduction to (12) leading (formally) to the system

$$\begin{aligned} -\Delta u &= 0 & \text{in } \Omega \subset \mathbb{R}^2, \\ \bar{u} &= g & \text{on } \Gamma, \\ u &= 0 & \text{on } \partial\Omega. \end{aligned} \quad (21)$$

We recall that \bar{u} computes a mean of function $u : \Omega \rightarrow \mathbb{R}$ over the curve $\Gamma = \Gamma_{\varepsilon}$, i.e. $\bar{u} = |\Gamma|^{-1} \int_{\Gamma} u$. Note that through u and \bar{u} the coupled problem (21) includes a dimensional gap of 2 (as in the case of $3d$ - $1d$ problem (3)).

Letting $V = H_0^1(\Omega)$ and $Q = \mathbb{R}$ the weak form of (21) reads: Find $u \in V, p_{\odot} \in Q$ such that

$$\begin{aligned} \int_{\Omega} \nabla u \cdot \nabla v - \int_{\Gamma} p_{\odot} \bar{v} &= 0 \quad \forall v \in V, \\ - \int_{\Gamma} q_{\odot} \bar{u} &= 0 \quad \forall q_{\odot} \in Q. \end{aligned} \quad (22)$$

For well-posedness of (22) when $\Gamma \subset \partial\Omega$ we refer to [12]. Here we shall consider Q with an inner product $(p_{\odot}, q_{\odot})_Q = \int_{\Gamma} p_{\odot} q_{\odot}$ inducing the norm $\|p_{\odot}\|_Q = (p_{\odot}, p_{\odot})_Q^{1/2}$. On V , the norm is given by the H^1 -seminorm. From the point of Brezzi theory a convenient property of the reduced problem is the fact that Q is one-dimensional. Thus, the Schur complement spectrum (18) contains just a single eigenvalue λ_B . Then, Figure 17 shows a computational evidence for

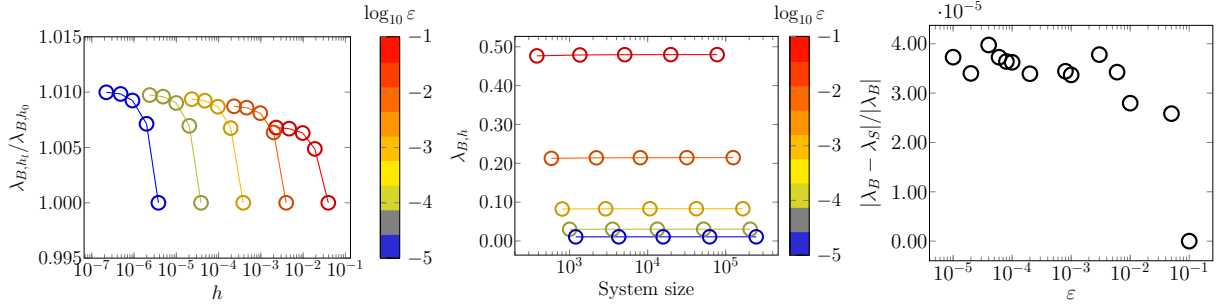


FIGURE 17. (Left, center) Mesh convergence of the Schur complement eigenvalue of (22) for $\Omega = \{x \in \mathbb{R}^2, |x| < 1\}$, $\Gamma_\varepsilon = \{x \in \Omega, |x| = \varepsilon\}$ and \mathbb{P}_1 elements. For each ε a sequence of problems is considered on uniformly refined meshes starting from size $h_0 \geq h_l \geq h_{\min}$ leading to eigenvalues λ_{B,h_l} . (Right) Error between the Schur complement eigenvalues and the eigenvalues of the Steklov problem (23). In both cases results for $h_l = h_{\min}$ are shown.

stability of (22) in $V \times Q$ with the chosen norms. Specifically, taking $\Omega = \{x \in \mathbb{R}^2 : |x| < 1\}$ such that the triangulation of the domain always conforms to Γ_ε , and using \mathbb{P}_1 elements, it can be seen that the Brezzi constant(s) related to the coupling operator⁶ are bounded in the mesh size. However, similar to the full problem (12) we observe that the numerical inf-sup/ B -boundedness constant λ_B decreases with radius ε , i.e. $\lambda_B = \lambda_B(\varepsilon)$.

As with the $2d$ - $1d$ problem we claim that λ_B is closely linked to a Steklov eigenvalue. In this case we consider: Find $u \in V$, $\lambda_S > 0$ satisfying

$$\int_{\Gamma} \bar{u}\bar{v} = \lambda_S^2 \int_{\Omega} \nabla u \cdot \nabla v \quad \forall v \in V. \quad (23)$$

From (23) it follows that the maximal eigenvalue λ_S relates to the estimates for the mean value of u on Γ_ε , that is,

$$\|\bar{u}\|_Q \leq \lambda_S \|u\|_V \quad \forall u \in V.$$

The relation between the two eigenvalues is demonstrated in Figure 17 which shows the relative error between the eigenvalues λ_B of the Schur complement of (22) and λ_S . Here only the values obtained on the finest meshes for each ε are considered, i.e. $\lambda_S = \lambda_{S,h_{\min}}$ and analogously for λ_B . In all the cases the observed error is $\sim 10^{-3}$.

Finally, in Figure 18 we measure the dependence of λ_S (and λ_B) on the radius ε . It can be seen that the relation is practically identical to that of the unreduced $2d$ - $1d$ problem (12), see also [19]. In particular, λ_B goes to 0 together with ε and the affect of inner radius on stability is not removed by model reduction.

In summary, we have established, through both numerical experiments and analytical expressions about the inf-sup and trace constant, a clear relationship between β and ε

$$\beta = C \sqrt{\varepsilon |\log \varepsilon|} \quad \text{as } \varepsilon \rightarrow 0 \quad (24)$$

with C a constant independent from ε . The result appears independent from the discretization parameters of the considered numerical framework, so that we can assert with reasonable confidence that such behaviour is inherent in the trace/extension operator structure of the interface problem.

5. CONCLUSION

The solvability of mixed-dimensional problems plays a crucial role in effectively applying these models to real-world scenarios, such as microcirculation. In our research, we have focused on operator preconditioning as a means to address this issue. We have demonstrated that by employing suitable weighted norms, the operator preconditioning framework can successfully

⁶The Brezzi conditions for the bilinear form a stemming from (22) are easily verified and the related constants take the value 1.

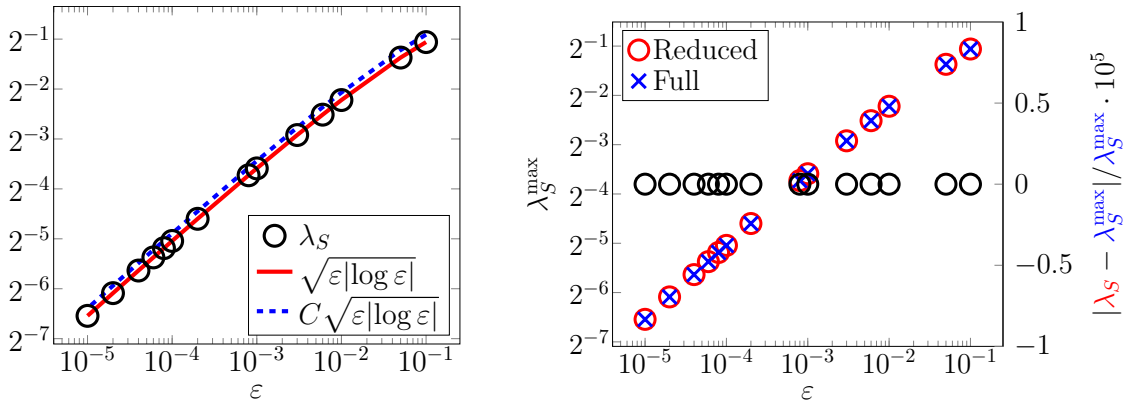


FIGURE 18. (Left) Dependence of the Steklov eigenvalue $\lambda_{S,h_{\min}}$ (black \circ markers) in (23) on the radius of coupling curve $\Gamma_\epsilon = \{x \in \Omega, |x| = \epsilon\}$. The constant $C \approx 0.999$ was optimized for best fit of the data. (Right) Comparison between the largest eigenvalues of the Steklov problems. The $2d$ - $1d$ problem (13) is related to (20) with eigenvalues $\lambda_S^{\max} = \lambda_{S,h_{\min}}^{\max}$ (blue \times markers), cf. Figure 13, while λ_S (red \circ markers) denotes eigenvalues of (23) related to $2d$ - $0d$ problem (22), see Figure 17. Relative error between the values of the full and reduced models is plotted against the right vertical axis in black \circ markers.

handle material parameters like diffusivity in both the $3d$ and $1d$ domains. However, when dealing with interface-coupled systems, these norms alone are insufficient to ensure robustness concerning geometric parameters, such as the inner radius. Through extensive numerical experiments, we have highlighted the significant impact of the parameter ϵ on the mathematical structure of the problem and its adverse effect on the well-posedness through the trace operator. It is worth noting that this behavior persists even in a non topologically-reduced framework. Therefore, the reduction of dimensionality and the use of appropriately scaled Sobolev spaces currently fail to guarantee the robustness of preconditioners as ϵ approaches zero. In our view, these findings strongly advocate for a thorough and fundamental analysis of the trace operator's role in coupling conditions within mixed-dimensional approaches. The ultimate goal is to develop a generalized trace operator capable of facilitating a robust coupling of partial differential equations across high-dimensional gaps.

REFERENCES

- [1] D. N. Arnold and M. E. Rognes. Stability of Lagrange elements for the mixed Laplacian. *Calcolo*, 46(4):245–260, 2009.
- [2] T. Blake and J. Gross. Analysis of coupled intra- and extraluminal flows for single and multiple capillaries. *Mathematical Biosciences*, 59(2):173–206, 1982.
- [3] D. Braess. Stability of saddle point problems with penalty. *ESAIM: Mathematical Modelling and Numerical Analysis-Modélisation Mathématique et Analyse Numérique*, 30(6):731–742, 1996.
- [4] F. Brezzi. On the existence, uniqueness and approximation of saddle-point problems arising from Lagrangian multipliers. *Publications mathématiques et informatique de Rennes*, (S4):1–26, 1974.
- [5] A. Budiša, X. Hu, M. Kuchta, K.-A. Mardal, and L. Zikatanov. Rational approximation preconditioners for multiphysics problems. In *International Conference on Numerical Methods and Applications*, pages 100–113. Springer, 2022.
- [6] D. Cerroni, F. Laurino, and P. Zunino. Mathematical analysis, finite element approximation and numerical solvers for the interaction of 3d reservoirs with 1d wells. *GEM-International Journal on Geomathematics*, 10:1–27, 2019.
- [7] C. D’Angelo. *Multi scale modelling of metabolism and transport phenomena in living tissues*, PhD Thesis. EPFL, Lausanne, 2007.
- [8] C. D’Angelo. Finite element approximation of elliptic problems with Dirac measure terms in weighted spaces: applications to one-and three-dimensional coupled problems. *SIAM Journal on Numerical Analysis*, 50(1):194–215, 2012.
- [9] C. D’Angelo and A. Quarteroni. On the coupling of 1d and 3d diffusion-reaction equations: Application to tissue perfusion problems. *Mathematical Models and Methods in Applied Sciences*, 18(08):1481–1504, 2008.

- [10] G. Fleischman, T. Secomb, and J. Gross. The interaction of extravascular pressure fields and fluid exchange in capillary networks. *Mathematical Biosciences*, 82(2):141–151, 1986.
- [11] G. Flieschman, T. Secomb, and J. Gross. Effect of extravascular pressure gradients on capillary fluid exchange. *Mathematical Biosciences*, 81(2):145–164, 1986.
- [12] L. Formaggia and C. Vergara. *Defective Boundary Conditions for PDEs with Applications in Haemodynamics*, pages 285–312. Springer International Publishing, Cham, 2018.
- [13] I. G. Gjerde, K. Kumar, and J. M. Nordbotten. A singularity removal method for coupled 1D–3D flow models. *Computational Geosciences*, pages 1–15, 2019.
- [14] G. Hartung, S. Badr, M. Moeini, F. Lesage, D. Kleinfeld, A. Alaraj, and A. Linninger. Voxelized simulation of cerebral oxygen perfusion elucidates hypoxia in aged mouse cortex. *PLoS Computational Biology*, 17(1):1–28, 01 2021.
- [15] J. Hersch, L. E. Payne, and M. M. Schiffer. Some inequalities for Stekloff eigenvalues. *Archive for Rational Mechanics and Analysis*, 57(2):99–114, 1974.
- [16] X. Hu, E. Keilegavlen, and J. M. Nordbotten. Effective preconditioners for mixed-dimensional scalar elliptic problems. *Water Resources Research*, 59(1):e2022WR032985, 2023.
- [17] T. Koch, K. Heck, N. Schröder, H. Class, and R. Helmig. A new simulation framework for soil–root interaction, evaporation, root growth, and solute transport. *Vadose Zone Journal*, 17(1), 2018.
- [18] T. Koch, M. Schneider, R. Helmig, and P. Jenny. Modeling tissue perfusion in terms of 1d-3d embedded mixed-dimension coupled problems with distributed sources. *Journal of Computational Physics*, 410:109370, 2020.
- [19] T. Köppl, E. Vidotto, B. Wohlmuth, and P. Zunino. Mathematical modeling, analysis and numerical approximation of second-order elliptic problems with inclusions. *Mathematical Models and Methods in Applied Sciences*, 28(05):953–978, 2018.
- [20] T. Köppl and B. Wohlmuth. Optimal a priori error estimates for an elliptic problem with Dirac right-hand side. *SIAM Journal on Numerical Analysis*, 52(4):1753–1769, 2014.
- [21] M. Kuchta. Assembly of multiscale linear PDE operators. In *Numerical Mathematics and Advanced Applications ENUMATH 2019*, pages 641–650. Springer, 2021.
- [22] M. Kuchta, F. Laurino, K.-A. Mardal, and P. Zunino. Analysis and approximation of mixed-dimensional PDEs on 3D-1D domains coupled with Lagrange multipliers. *SIAM Journal on Numerical Analysis*, 59(1):558–582, 2021.
- [23] M. Kuchta, K.-A. Mardal, and M. Mortensen. Preconditioning trace coupled 3d-1d systems using fractional Laplacian. *Numerical Methods for Partial Differential Equations*, 0(0).
- [24] M. Kuchta, M. Nordaas, J. Verschaeve, M. Mortensen, and K. Mardal. Preconditioners for saddle point systems with trace constraints coupling 2d and 1d domains. *SIAM Journal on Scientific Computing*, 38(6):B962–B987, 2016.
- [25] T. Köppl, E. Vidotto, B. Wohlmuth, and P. Zunino. Mathematical modeling, analysis and numerical approximation of second-order elliptic problems with inclusions. *Mathematical Models and Methods in Applied Sciences*, 28(5):953–978, 2018.
- [26] Laurino, F. and Zunino, P. Derivation and analysis of coupled PDEs on manifolds with high dimensionality gap arising from topological model reduction. *ESAIM: M2AN*, 53(6):2047–2080, 2019.
- [27] A. Linninger and T. A. Ventimiglia. Mesh-free high-resolution simulation of cerebrocortical oxygen supply with fast Fourier preconditioning. *bioRxiv*, pages 2023–01, 2023.
- [28] J. L. Lions and E. Magenes. *Non-homogeneous boundary value problems and applications: Vol. 1*, volume 181. Springer Science & Business Media, 2012.
- [29] A. Logg, K.-A. Mardal, G. N. Wells, et al. *Automated Solution of Differential Equations by the Finite Element Method*. Springer, 2012.
- [30] K.-A. Mardal and R. Winther. Preconditioning discretizations of systems of partial differential equations. *Numerical Linear Algebra with Applications*, 18(1):1–40, 2011.
- [31] M. F. Murphy, G. H. Golub, and A. J. Wathen. A note on preconditioning for indefinite linear systems. *SIAM Journal on Scientific Computing*, 21(6):1969–1972, 2000.
- [32] J. Nečas. *Direct methods in the theory of elliptic equations*. Springer Science & Business Media, 2011.
- [33] D. Peaceman. Interpretation of well-block pressures in numerical reservoir simulation. *Soc Pet Eng AIME J*, 18(3):183–194, 1978.
- [34] D. W. Peaceman. Interpretation of well-block pressures in numerical reservoir simulation with nonsquare grid blocks and anisotropic permeability. *Society of Petroleum Engineers journal*, 23(3):531–543, 1983.
- [35] J. Qin. *On the convergence of some low order mixed finite elements for incompressible fluids*. The Pennsylvania State University, 1994.
- [36] M. E. Rognes. Automated testing of saddle point stability conditions. In *Automated Solution of Differential Equations by the Finite Element Method: The FEniCS Book*, pages 657–671. Springer, 2012.
- [37] T. Rusten and R. Winther. A preconditioned iterative method for saddlepoint problems. *SIAM Journal on Matrix Analysis and Applications*, 13(3):887–904, 1992.
- [38] Y. Saad. *Iterative methods for sparse linear systems*. SIAM, 2003.

- [39] T. Secomb, R. Hsu, E. Park, and M. Dewhirst. Green's function methods for analysis of oxygen delivery to tissue by microvascular networks. *Annals of Biomedical Engineering*, 32(11):1519–1529, 2004.
- [40] O. Steinbach. *Numerical approximation methods for elliptic boundary value problems: finite and boundary elements*. Springer Science & Business Media, 2007.

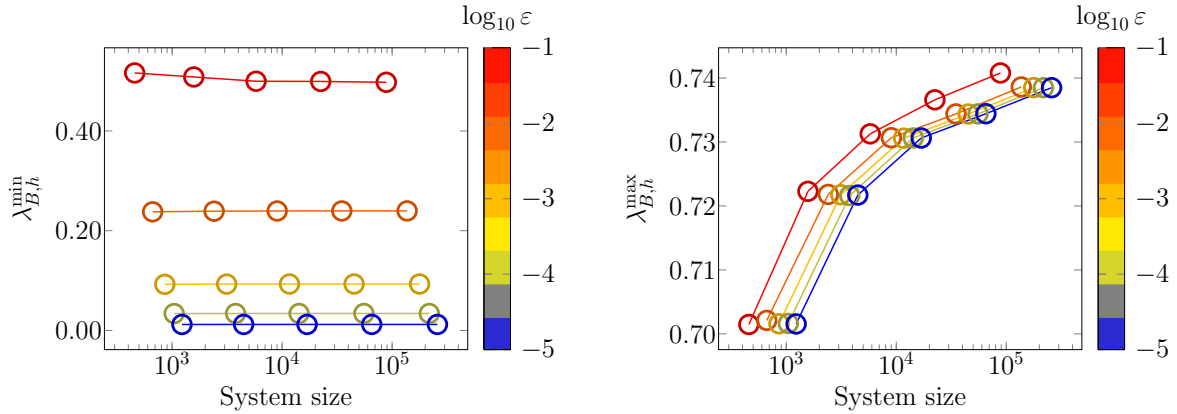


FIGURE 19. (Left) Mesh convergence of the extremal eigenvalues of Schur complement (18) for $\Omega = (-1, 1)^2$, $\Gamma_\varepsilon = \partial(-\varepsilon, \varepsilon)^2$. Both spaces V and Q are discretized by \mathbb{P}_1 elements. For each ε a sequence of problems is considered on uniformly refined meshes starting from size $h_0 \geq h_l \geq h_{\min}$ leading to eigenvalues λ_{B, h_l} .

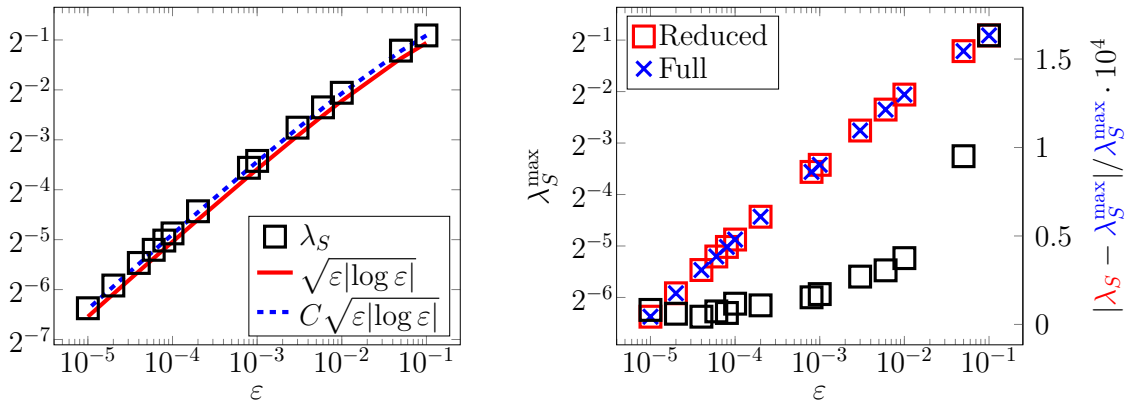


FIGURE 20. Dependence of the Steklov eigenvalue $\lambda_{S, h_{\min}}$ in (23) on the radius of coupling curve $\Gamma_\varepsilon = \partial(-\varepsilon, \varepsilon)^2$. The constant $C \approx 1.116$ was optimized for best fit of the data. (Right) Comparison between the largest eigenvalues of the Steklov problems. The $2d-1d$ problem (13) is related to (20) with eigenvalues $\lambda^{\max} = \lambda_{S, h_{\min}}^{\max}$, cf. Figure 13, while λ_S denotes eigenvalues of (23) related to $2d-0d$ problem (22), see Figure 17. Relative error between the values of the full and reduced models is plotted against the right vertical axis in black \square markers.

APPENDIX A. APPENDIX

A.1. Numerical experiments for square-shaped inclusion. For the sake of comparison of the effect of the inclusion shape on the relation between well-posedness of (13) and the diameter of the inclusion we collect here additional results for $\Gamma_\varepsilon = \partial(-\varepsilon, \varepsilon)^2$ and $\Omega = (-1, 1)^2$. These results are analogous to Figure 12 and Figure 18 where circular Γ_ε is considered.

A.2. Numerical experiments for layered mesh. Here we collect additional results regarding the numerical experiments for a circular domain $\Omega = \{x \in \mathbb{R}^2, |x| < 1\}$ with circular inclusion $\Gamma_\varepsilon = \{x \in \Omega, |x| = \varepsilon\}$ obtained on layered mesh (see Figure 15 (right)) conformal simultaneously to every Γ_{ε_i} , with $\varepsilon_i \in \{10^{-1}, 10^{-2}, 10^{-3}, 10^{-4}, 10^{-5}\}$.

A.3. Numerical experiments for $\mathbb{P}_2 - \mathbb{P}_1$ discretization.

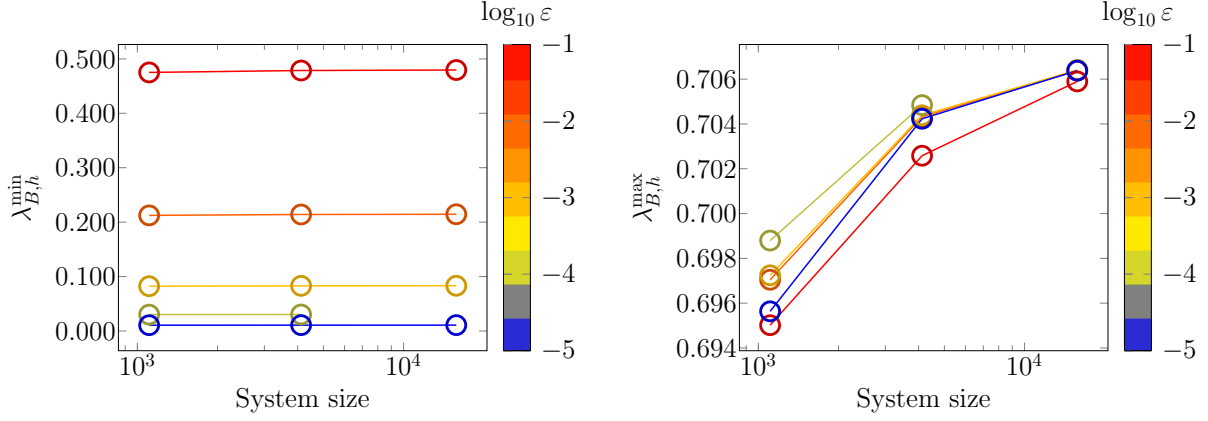


FIGURE 21. (Left) Mesh convergence of the extremal eigenvalues of Schur complement (18) for $\Omega = \{x \in \mathbb{R}^2, |x| < 1\}$, $\Gamma_\varepsilon = \{x \in \Omega, |x| = \varepsilon\}$. Both spaces V and Q are discretized by \mathbb{P}_1 elements. For each ε a sequence of problems is considered on uniformly refined layered mesh starting from size $h_0 \geq h_l \geq h_{\min}$ leading to eigenvalues λ_{B,h_l} .

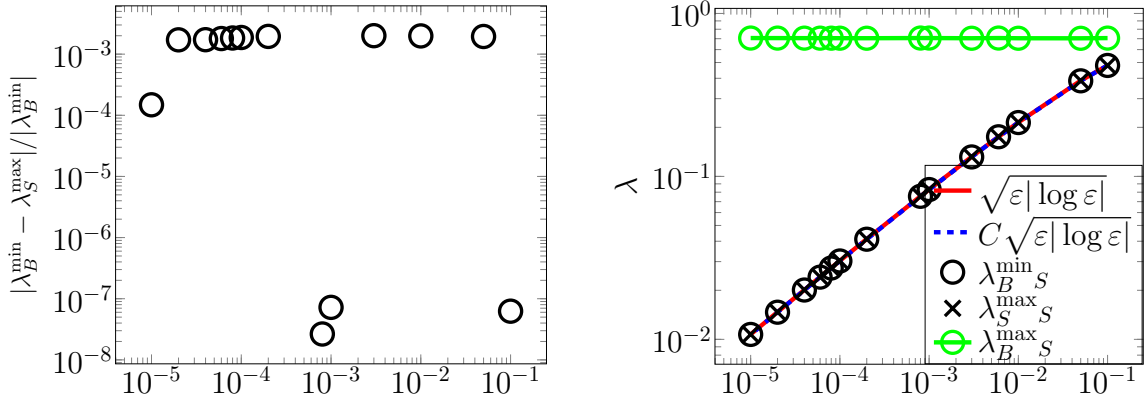


FIGURE 22. Error between the smallest eigenvalue λ_B^{\min} of the Schur complement problem (18) and the largest eigenvalue λ_S^{\max} of the Steklov problem (20). In both cases, values from the finest level of refinement are considered, i.e. $\lambda_X := \lambda_{X,h_{\min}}$. (Right) Dependence of eigenvalues from the radius of coupling curve $\Gamma_\varepsilon = \{x \in \Omega, |x| = \varepsilon\}$. Value $C \approx 0.999$ is obtained by fitting values λ_B^{\min} for $\varepsilon < 10^{-1}$.

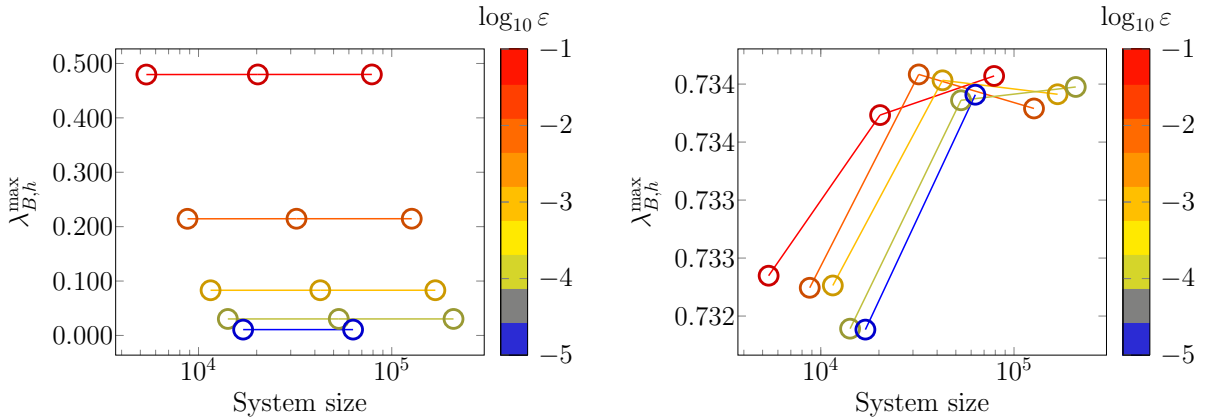


FIGURE 23. (Left) Mesh convergence of the extremal eigenvalues of Schur complement (18) for $\Omega = \{x \in \mathbb{R}^2, |x| < 1\}$, $\Gamma_\varepsilon = \{x \in \Omega, |x| = \varepsilon\}$. Spaces V and Q are discretized respectively by \mathbb{P}_2 and \mathbb{P}_1 elements. For each ε a sequence of problems is considered on uniformly refined meshes starting from size $h_0 \geq h_l \geq h_{\min}$ leading to eigenvalues λ_{B,h_l} .

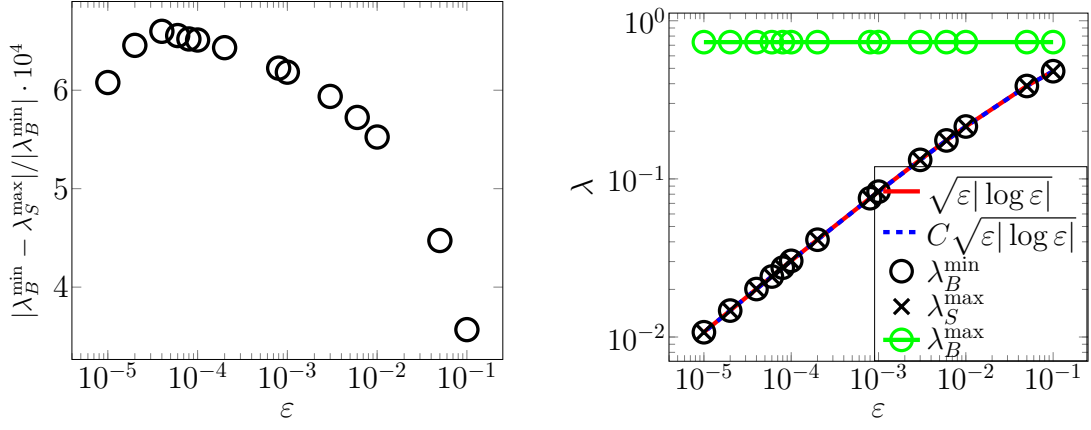


FIGURE 24. Error between the smallest eigenvalue λ_B^{\min} of the Schur complement problem (18) and the largest eigenvalue λ_S^{\max} of the Steklov problem (20). In both cases, values from the finest level of refinement are considered, i.e. $\lambda_X := \lambda_{X,h_{\min}}$. (Right) Dependence of eigenvalues from the radius of coupling curve $\Gamma_\varepsilon = \{x \in \Omega, |x| = \varepsilon\}$. Value $C \approx 0.999$ is obtained by fitting values λ_B^{\min} for $\varepsilon < 10^{-1}$.